

POLYMER TRIMERS AS BUILDING BLOCKS FOR PHOTONICS

A Thesis

Presented to the Faculty of the Graduate School

of Cornell University

In Partial Fulfillment of the Requirements for the Degree of

Master of Science

by

Trina Ghosh Dastidar

May 2010

© 2010 Trina Ghosh Dastidar

ABSTRACT

Self-assembled photonic materials provide an important low cost route to light control. Particularly, crystals that exhibit an omnidirectional photonic band gap for light waves have been sought for use in LED out-coupling applications, zero threshold semiconductor lasers, sensors with very low detection limits, and high efficiency solar cells. The general class of photonic crystal materials is constructed to have periodic dielectric constant and high dielectric contrast between building blocks and matrix regions. The width and stability of an optical band gap in photonic crystals strongly depends on the lattice and basis of the structures.

Spherical colloidal particles have dominated the research on this topic in colloidal science. However, nonspherical motifs have been shown in theoretical reports to more effectively promote strong light-matter interactions leading to the desired control of dispersion properties. Work on the synthesis of monodisperse colloidal particles in a range of shapes, micron and submicron sizes, composition and surface characteristics has intensified in recent years. However, it still remains a challenge to produce ordered arrays over large areas with nonspherical particles.

In the present work, monodisperse 'bent' trimer polystyrene colloids 1-2 μm in largest dimension were synthesized using multi-stage seeded emulsion polymerization. The seed crosslinking density, hydrophilic coating density and swelling ratio of monomer to polymer were varied to obtain uniform particles. The spontaneous organization of the trimer building blocks under confinement was examined using optical and confocal microscopy. Monolayer films with particle axes oriented in-plane, out-of-plane, or at

acute angles with respect to the substrate were observed in the wedge cell confinement geometry as a function of cell height and particle morphology.

BIOGRAPHICAL SKETCH

Trina Ghosh Dastidar was born in the city of joy, Kolkata, India in the year of 1984. As the only female child of a Bengali middle class family she was brought up in a strict but friendly atmosphere. Inspired by her father's devotion towards science she developed a yearning for knowledge and passion for reading and learning at a very young age. Unlike a lot of Indian females who are not encouraged to go after their dreams, her family always supported her goal to make a contribution towards science. Under the care and attention of parents and teachers she managed to excel in her field of study, Chemistry, and decided to pursue higher education. The concept of interdisciplinary research to her was extremely fascinating and she aspired to work on interdisciplinary chemistry and material science in a premier university to gradually carve out a niche for herself in the scientific community. This brought her to the department of Material Science and Engineering, Cornell University in the spring of 2007.

ACKNOWLEDGMENTS

I thank my advisor, Prof. Chekesha Liddell, for the opportunity to work on this interesting topic and for her support, enthusiasm and knowledge in guiding me. Her unending energy level was always a great motivation. I would like to thank Prof. Richard Hennig and Prof. Anil Netravali for their encouragement and support.

I acknowledge support, help, and feedback from my colleagues in the Liddell group. I thank the Cornell Center for Material Science (CCMR) and Cornell Nano Fabrication (CNF) facility managers for their assistance in microscope imaging and other training. I also thank Carol Bayels for her help in confocal imaging. I am thankful to the Cohen group members for sharing lab-space and the Cohen group optical microscope with me.

Finally, I thank my parents for their infinite and unconditional support.

Trina Ghosh Dastidar

Cornell University

18th January 2010

TABLE OF CONTENTS

BIOGRAPHICAL SKETCH	iii
ACKNOWLEDGMENTS	iv
TABLE OF CONTENTS	v
LIST OF FIGURES	vii
LIST OF TABLES	xi
Chapter 1	1
1 Introduction.....	1
1.1 Photonic Crystals.....	1
1.2 Nonspherical Colloids as Building Blocks for Photonic Crystals.....	2
1.3 Synthesis and Assembly of Nonspherical Colloids.....	4
1.4 Shape Anisotropic Particles.....	5
1.5 Chemically Anisotropic Particles.....	9
1.6 Assembly of Anisotropic Colloids	11
1.7 Convective Assembly of Colloidal Particles	13
1.8 Confinement Technique	14
Chapter 2	17
2 Results and Discussions.....	17

2.1 Synthesis of Linear Polystyrene Particles Using the Dispersion Polymerization	
Method	17
2.2 Synthesis of Crosslinked Polystyrene Particles Using a Seeded Emulsion	
Polymerization Technique.....	17
2.3 Synthesis of Anisotropic Dimer -Shaped Particles by Protrusion of Daughter Lobe	
from CLPS.....	18
2.4 Synthesis of Trimer Shaped Particles from Parent Dimer Particles.....	20
2.5 Silica Coating of Dimer and Trimer Polystyrene Building Block.....	29
2.6 Self-assembly Under Confinement	31
Chapter 3.....	37
3 Summary and Future Directions	37
APPENDIX	39
REFERENCES	41

LIST OF FIGURES

Figure 1.1	Dispersion diagram for an FCC crystal composed of spherical particles	2
Figure 1.2	Diamond-type crystal structure produced by replacing spherical building blocks in an FCC crystal with dimers.....	3
Figure 1.3	Band diagram for a complete photonic band gap material with a diamond lattice based on dimer.....	4
Figure 1.4	Ellipsoidal polystyrene particles of different aspect ratios produced by stretching spherical polystyrene particles. Scheme A yields ellipsoids, while B yields ‘barrels’.....	5
Figure 1.5	Inorganic particle shapes produced from ferric chloride using gel-sol method.....	6
Figure 1.6	Synthesis of dimer ‘dumbbell’ from crosslinked sphere by seeded emulsion polymerization	7
Figure 1.7	Rugby ball and red blood cell polymer shapes synthesized from PS spheres. Insets indicate the ratio of crosslinking reagent to monomer.	8
Figure 1.8	A) Triple rod, B) triangular, C) ice cream cone, and D) diamond particles produced by multi-step seeded polymerization.	8
Figure 1.9	Patchy particles via colloids added to oil-in-water emulsions.....	9
Figure 1.10	Trimers synthesized by adsorption of silica particles onto patchy particles.	10

Figure 1.11	Continuous flow lithographic technique to produce Janus particles	11
Figure 1.12	2D hard spherocylinders with a transition from A) a solid structure characterized by localized particle chaining and B) a smectic liquid crystal phase.....	12
Figure 1.13	A) Phase diagram of dimer system. Shaded area indicates two phase regions for the first order phase transitions. B) Dimers in a close-packed degenerate crystal arrangement.	12
Figure 1.14	Simulation results for A) fluid, B) rotator and C) crystal phases formed by pentamer building blocks. Grey scale indicates similarly oriented pentamers.....	13
Figure 1.15	Convective assembly of spherical colloids.....	14
Figure 1.16	Confinement of colloidal particles and formation of uniform geometry clusters between two glass substrates of a fluidic cell.....	15
Figure 1.17	A) Confinement cell. B) Polystyrene beads packing in V-grooves of the substrate in A). C) FCC crystal with (100) lattice plane orientation as the top surface	16
Figure 1.18	A) Wedge cell construction for confinement-assisted assembly of dimers. B) Rotator and C) hexagonal phase of dimers under confinement	16
Figure 2.1	A) Linear polystyrene and B) crosslinked polystyrene particles.	18
Figure 2.2	Schematic of monomer droplet adsorbed onto the crosslinked particle, compelling lobe interpenetration by the ‘dynamic swelling method’	19

Figure 2.3	Schematic showing states of expulsion of monomer from CLPS A) complete wetting B) mild wetting C) negligible wetting D) zero wetting...	20
Figure 2.4	Schematic protrusion of third lobe from dimers in line with the parent lobes to produce A) straight particles (linear growth) and B) perpendicular to the parent lobes (perpendicular growth)	21
Figure 2.5	Experimental schemes for synthesis of trimers.	23
Figure 2.6	Dimers synthesized from CLPS A) 25% DVB $\sigma = 4$, B) 25% DVB $\sigma = 2$, C) 30% DVB $\sigma = 4$ and D) 30% DVB $\sigma = 2$	24
Figure 2.7	Trimers synthesized with a swelling ratio of A) 2:1, B) 3:1, C) 3:1 (straight trimer, enlarged view), D) 3:1 (angular trimer, enlarged view), E) 4:1, F) 4:1 (straight trimer, enlarged view), G) 4:1 (angular trimer, enlarged view) and F) 5:1.....	26
Figure 2.8	Increase in third lobe diameter with monomer to polymer swelling ratio..	27
Figure 2.9	Trimers synthesized from A) dimer seed particles (30% DVB, $\sigma=4$) with coating density, $\sigma=0$; B) dimer seed particles (30% DVB, $\sigma=2$) with coating density $\sigma=2$	28
Figure 2.10	A) Rhodamine isothiocyanite (RITC), B) 3-aminopropyltriethoxysilane (APS) C) APS-RITC complex.	30
Figure 2.11	Fluorescence micrographs of A) silica coated dimers and B) silica coated trimers.	30
Figure 2.12	A) Bare and B) silica coated dimer building blocks for assembly.	31

Figure 2.13	Monte Carlo (MC) simulation of self-assembly of trimer building blocks with functional lobe. A) Low density fluid phase and B) high density ordered structure of trimers.....	31
Figure 2.14	A, B) 2D projection map of crystal form 1 (c2mm plane group). C, D) 2D projection map of crystal form 2 (p3 plane group). E, F) 2D projection map of crystal form 3 (p6 plane group)	32
Figure 2.15	Wedge cell constructions for asymmetric dimers showing variation of particle orientation and ordering with gradient in height	33
Figure 2.16	Optical micrograph of A) edge of in-plane monolayer phase, B) high density monolayer phase, C) out-of-plane monolayer phase and D) multilayered phase.	34
Figure 2.17	A) Confocal images of in-plane monolayer. B) Autocorrelation for in-plane monolayer phase. C) FFT of in-plane monolayer. D) Confocal micrograph of trimers oriented out-of-plane. E) Autocorrelation of out-of-plane oriented trimers. F) FFT of out-of-plane monolayer.....	35
Figure 2.18	Intermediate phase for z-height between that of the in-plane and out-of-plane oriented structures for silica-coated trimers (2.12B).....	36

LIST OF TABLES

Table 2.1	Shape parameters for nonspherical polystyrene particles.	29
------------------	---	----

Chapter 1

1 Introduction

1.1 Photonic Crystals

Photonic crystals (PCs) are materials with high refractive index regions, which are spatially ordered. The periodic potentials in a subset of these composite structures give rise to photonic band gaps. Such artificial crystals block the propagation of light in particular frequency ranges, irrespective of the direction and polarization of the waves. The effect is analogous to that of band gaps in semiconductor materials, where the propagation of electrons is forbidden for electron energy between the conduction and valence band values. Tailoring the dispersion and band gap properties of photonic crystals thus offers a novel means to control light.¹

The photonic band structure of a crystal is determined by solving the wave equation that is derived from Maxwell's equations to obtain dispersion relations, $\omega(\mathbf{k})$. A dispersion diagram for a face-centered cubic (FCC) crystal of spheres is provided in Figure 1.1. The allowed modes for wave propagation are represented by the energy (or normalized inverse wavelength, y-axis) and the reciprocal lattice vector (x-axis). The inset showing the first Brillouin zone depicts the relationship between the high symmetry planes of the crystal and the direction of light travel.²

There is no complete photonic band gap for the case provided in Figure 1.1. In fact, PCs with full omnidirectional gaps have been difficult to fabricate. The crystal structure, refractive index contrast (n_c) between high- and low index regions, filling

fraction of high index materials, as well as the symmetry at lattice points must be tuned to obtain materials with complete PBGs or to increase the width of partial PBGs.³

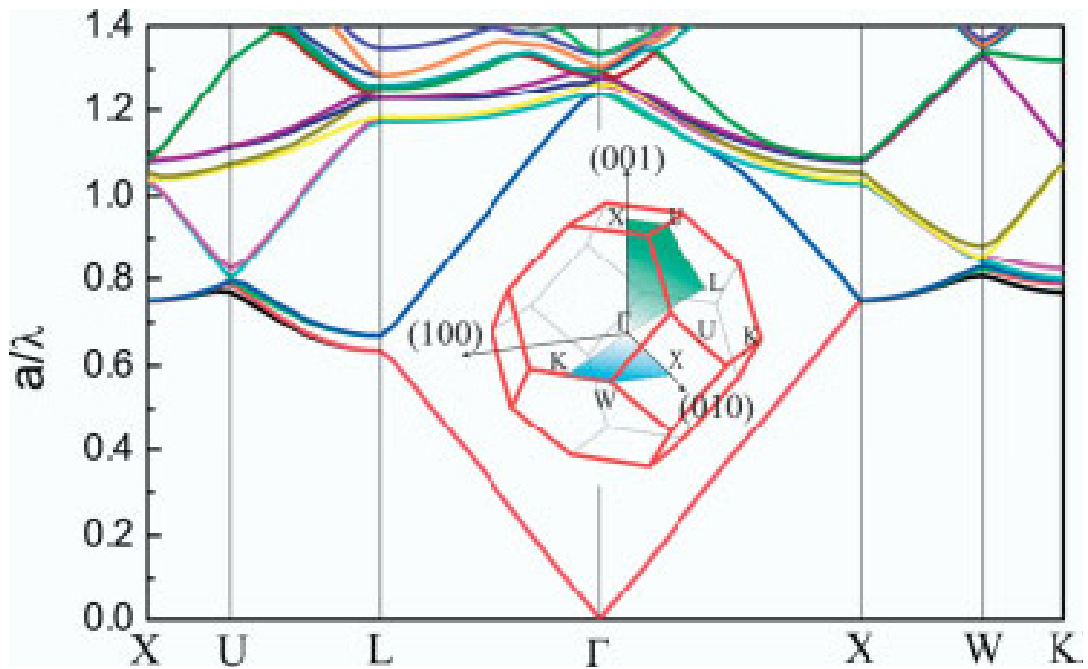


Figure 1.1 Dispersion diagram for an FCC crystal composed of spherical particles.²

1.2 Nonspherical Colloids as Building Blocks for Photonic Crystals

In order to obtain complete PBGs by the symmetry reduction strategy, nonspherical colloidal particles have been sought as building blocks for photonic crystal structures. Colloids in this context belong to the particle size range between a hundred nanometers and a few microns. When the particles are dispersed in a liquid medium they show characteristic Brownian and thermal motion.

Emulsion polymerization techniques have been used to synthesize spherical colloids in copious quantities with uniform shape and size. The highly monodisperse spherical particles self-assemble to form long range, ordered arrays. The periodic lattices

in two or three dimensions have the ability to diffract light waves. Such studies of the light scattering power of spherical colloids have increased our understanding of photonic crystals and PBG materials. However, as illustrated by the dispersion diagram in Figure 1.1, spherical colloids are not the most suitable building blocks for fabricating photonic crystals with a complete band gap. Specifically, there is degeneracy at the W- and U-points for the photonic band structure in Figure 1.1.

Theoretical studies have indicated that the degeneracy is lifted when the spheres in the FCC lattice are replaced by dimers (two dielectric spheres in contact, Figure 1.2). The resulting diamond-type lattice shows a complete band gap between the second and third bands, as shown in Figure 1.3. The gaps were tuned to open and close by controlling the dimer orientation. As an embodiment, peanut-shaped particles of ferric oxide ($n_c = 3.01$) on an FCC lattice were predicted to give rise to a photonic band gap that extends throughout the entire Brillouin zone. Though desired band gap properties are expected for such arrangements, the prediction of which structures actually form based on thermodynamic considerations remains an open question.^{4,5}

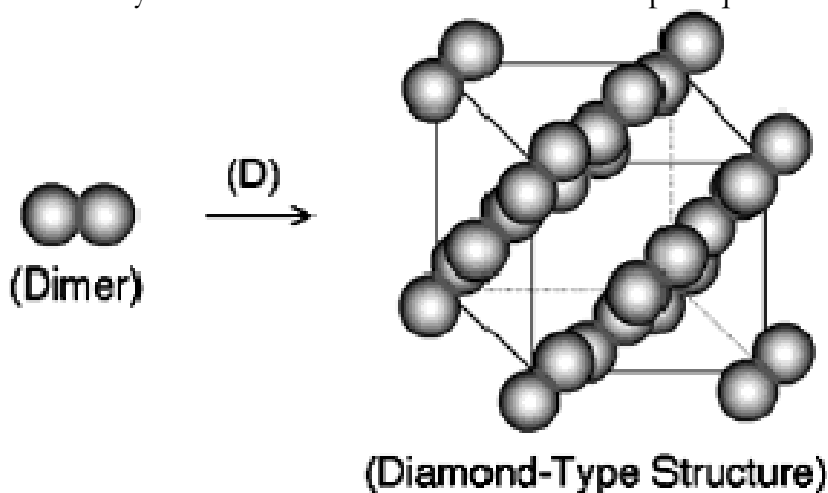


Figure 1.2 Diamond-type crystal structure produced by replacing spherical building blocks in an FCC crystal with dimers.⁴

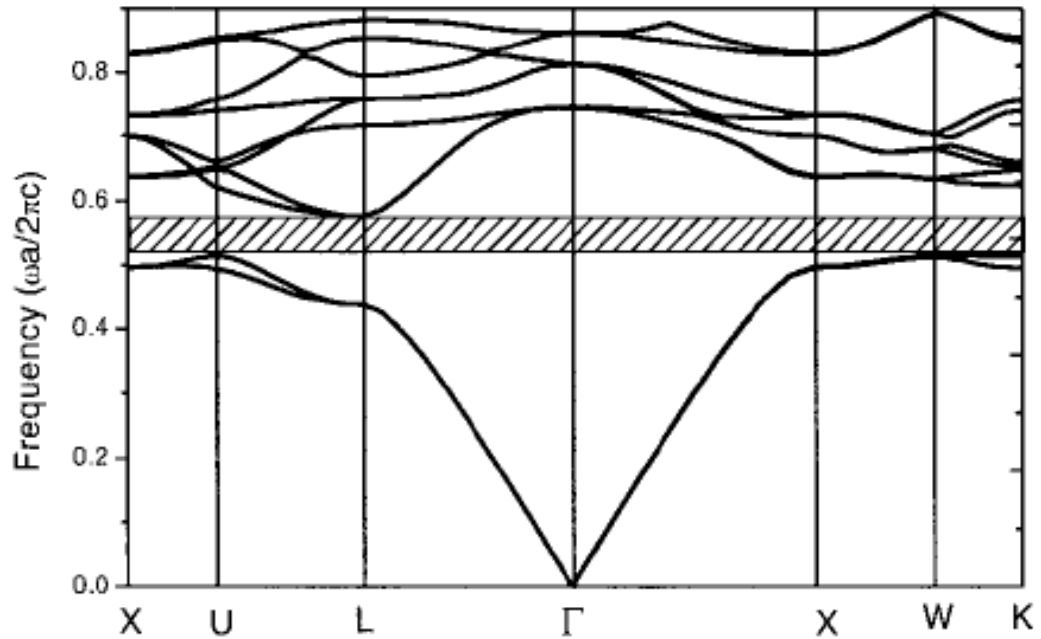


Figure 1.3 Band diagram for a complete photonic band gap material with a diamond lattice based on dimers.⁴

Simulations have been conducted by a number of research groups to predict a relationship between complex morphology motifs and the crystalline or unconventionally ordered solid phases that could be expected to assemble from the particles.⁶⁻⁸ Nonspherical colloids have also been discussed as mimics of diatomic molecules, short chain paraffins and water molecules that could provide insight into liquid-glass transition and crystallization, since the molecular details themselves are more difficult to study directly. For photonics, the major challenge is to synthesize monodisperse colloids in sufficient quantity and to control their assembly over large areas.⁴

1.3 Synthesis and Assembly of Nonspherical Colloids

Several of the techniques that have been developed in recent years for the synthesis and assembly of anisotropic particles are discussed in what follows. The

strategies include sphere deformation, precipitation, daughter lobe growth, sphere collapse, aggregation and templating.

1.4 Shape Anisotropic Particles

Spherical polystyrene particles were embedded in a matrix of polyvinyl alcohol (PVA) and heated above their glass transition temperature. The composite was stretched and then rapidly cooled to resolidify, as shown schematically in Figure 1.4. Dissolution of PVA yielded free ellipsoidal polymer bead shapes. The aspect ratio of the ellipsoidal colloids was varied by deforming latex of different sizes and by adjusting the strain rate.⁹

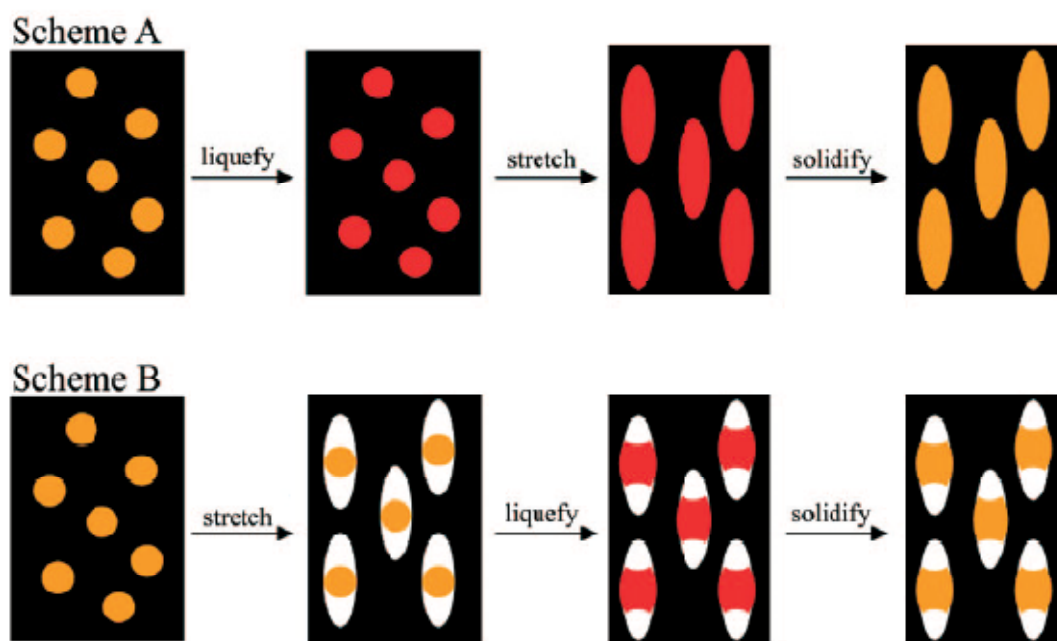


Figure 1.4 Ellipsoidal polystyrene particles of different aspect ratios produced by stretching spherical polystyrene particles. Scheme A yields ellipsoids, while B yields ‘barrels’.⁹

Inorganic ellipsoidal shapes were prepared using the gel-sol method from ferric chloride and sodium hydroxide reagents. The particle morphology was determined by the concentration of the shape-controlling anions, for example, sulfate, phosphate and chloride. The aging time also modified the shape and size of the particles. Cubic, rod-like, ellipsoidal, spindle and peanut shapes have been reported (Figure 1.5).¹⁰

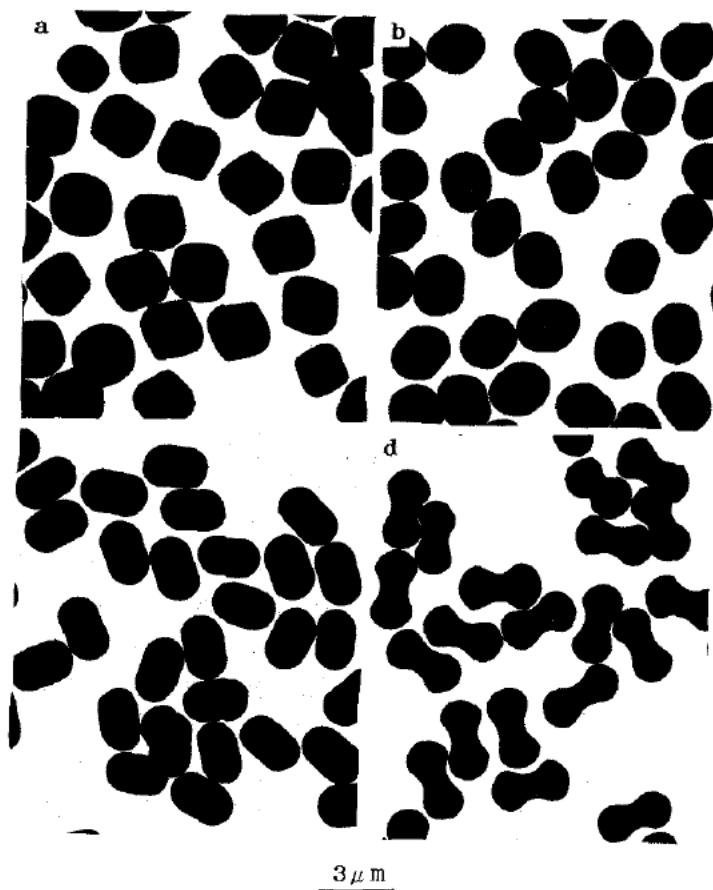


Figure 1.5 Inorganic particle shapes produced from ferric chloride using gel-sol method.¹⁰

Nonspherical particles of various functional materials have also been made by templating the gel-sol synthesized fine particles. Hollow silica or titania peanut shaped particles were produced by coating hematite and etching out the core. Polypyrrrole

ellipsoidal shells were grown by adding a silica primer layer onto hematite colloids.¹¹ Dumbbell-shaped polymer particles (Figure 1.6) have also been synthesized using a seeded emulsion polymerization technique. The shape may be varied by tuning the crosslinking density¹² or hydrophilic coating on the seed particles,¹³ as well as the monomer to polymer swelling ratio. Thermodynamic and kinetic aspects of the process of swelling the polymer with monomer additionally control the degree of protrusion of secondary lobes.^{12, 13}

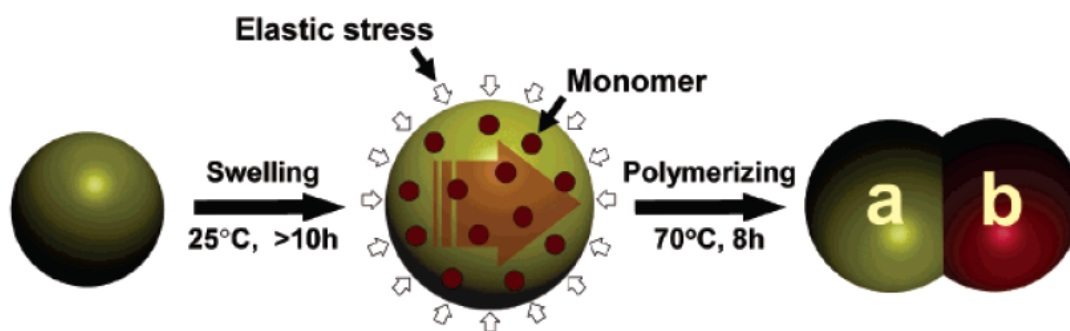


Figure 1.6 Synthesis of dimer ‘dumbbell’ from crosslinked sphere by seeded emulsion polymerization.¹²

Rugby ball and red blood corpuscle shaped polymer particles have been synthesized from PS spheres swollen with divinylbenzene, vinyltoluene and xylene utilizing the dynamic swelling method.^{14, 15} Figure 1.7 shows the range of dimpled morphology that occurs as the interior solvent escapes and the particles collapse.

More complex polymer shapes, for example ‘ice cream cones’ and ‘triangular’ (Figure 1.8), have been prepared via a stepwise seeded polymerization procedure by

carefully manipulating the crosslinking density gradient to direct the angle at which the third lobe is expelled.¹⁶

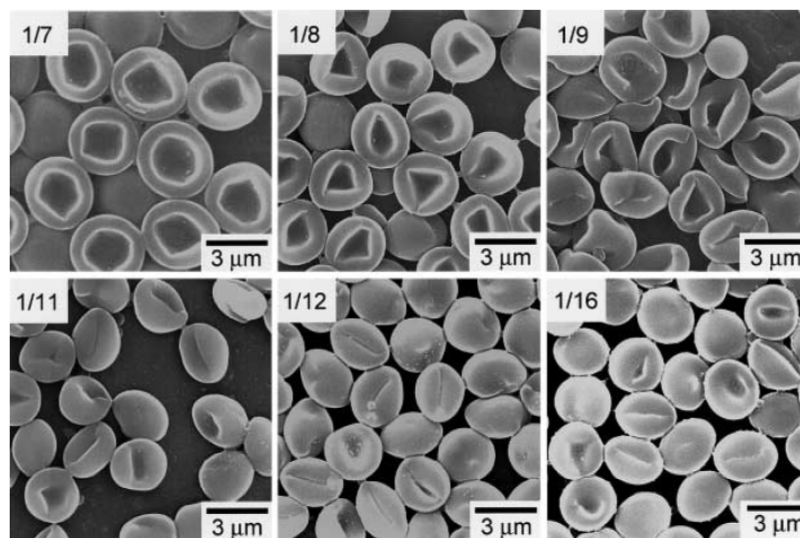


Figure 1.7 Rugby ball and red blood cell polymer shapes synthesized from PS spheres. Insets indicate the ratio of crosslinking reagent to monomer.¹⁴

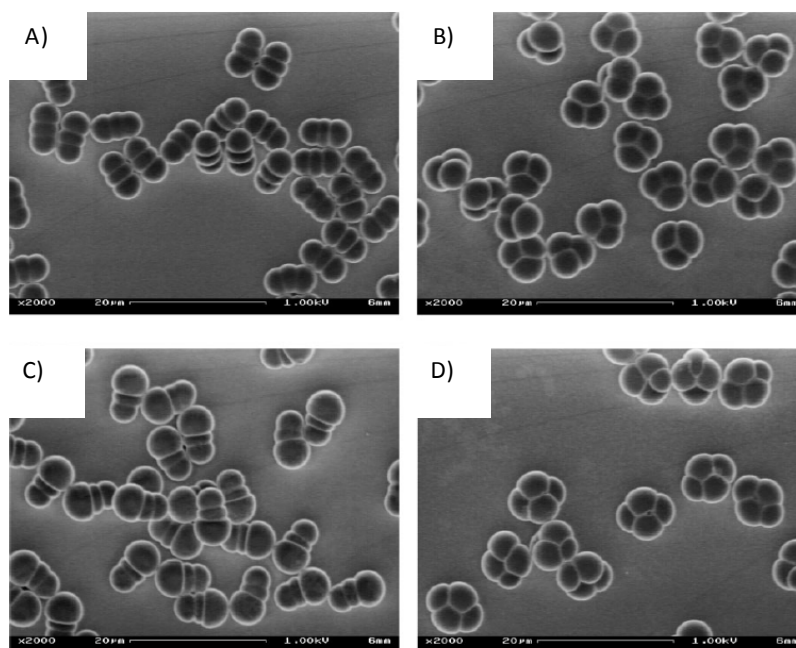


Figure 1.8 A) Triple rod, B) triangular, C) ice cream cone, and D) diamond particles produced by multi-step seeded polymerization.¹⁶

1.5 Chemically Anisotropic Particles

In addition to shape anisotropy, chemical anisotropy has also been achieved in colloidal particle synthesis. ‘Dipolar’ dumbbells, two-faced or surface anisotropic Janus particles, and locally functionalized patchy particles have been synthesized.

Dipolar dumbbells. Dumbbell-shaped particles with a PMMA daughter lobe have been prepared using PS seeds and methyl- or butylmethacrylate (MMA) as the monomers during the swelling steps of the seeded emulsion polymerization process.¹²

Patchy particles. PS or silica microspheres have been dispersed with linear homopolymers or nanoparticles into the oil droplets of an oil-in-water emulsion. For instance, the PS homopolymers partially cover the PS microspheres, leading to the well-organized patches shown in Figure 1.9. Composite clusters were prepared by the addition of organosilica or gold nanoparticles. Selective removal of the PS microspheres from the composite particles produced silica or gold colloidal aggregates with a defined arrangement of large pores.¹⁷

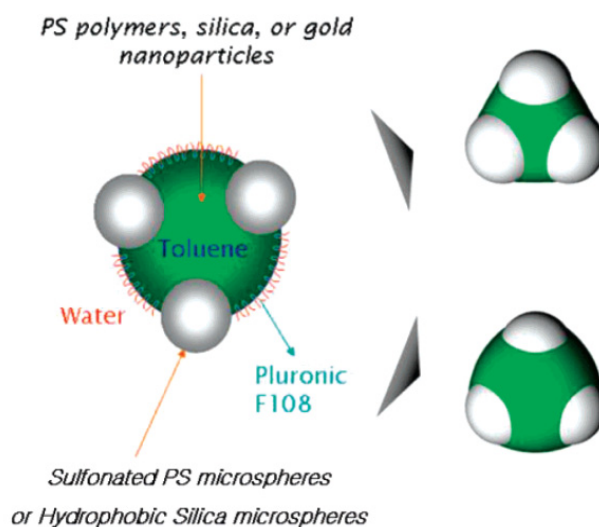


Figure 1.9 Patchy particles via colloids added to oil-in-water emulsions.¹⁷

In another approach, silica core particles were aggregated into doublets by a salting out technique and were coated with sulfate functionalized PS nanoparticles. Doublets were electrostatically bound to the surface of a Petri dish so that particle-particle and particle-substrate contact points were devoid of the coating. Excess unfunctionalized silica particles were added to singlets freed from the doublets under sonication. These attached to the patchy particles resulting in trimer shaped particle aggregates, as shown in Figure 1.10.¹⁸

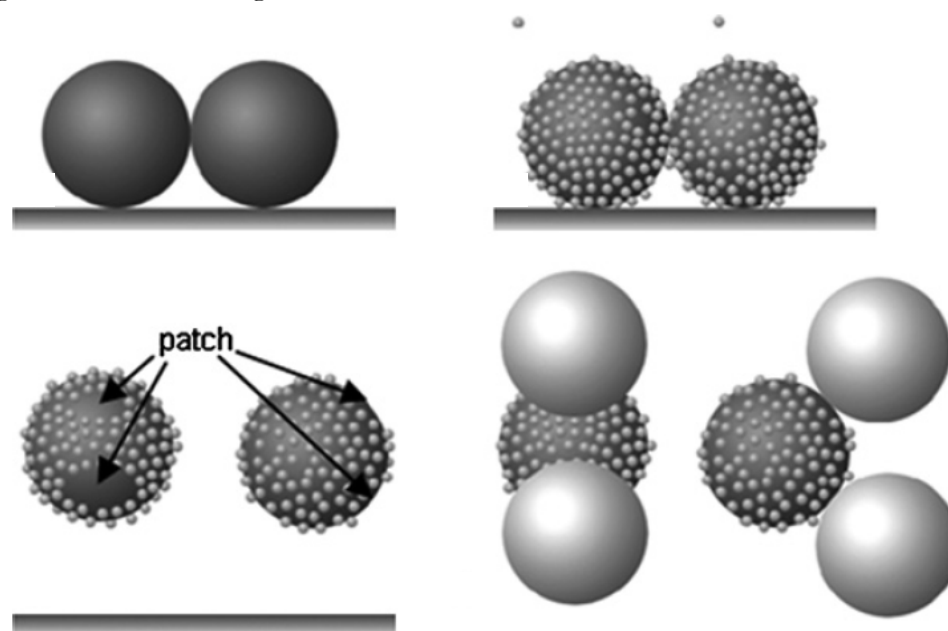


Figure 1.10 Trimers synthesized by adsorption of silica particles onto patchy particles.¹⁸

Janus particles. Continuous flow lithography has been employed to produce Janus colloids and other complex particles. In the process, poly(ethyleneglycol)diacrylate (PEG-DA) oligomer was passed through a polydimethylsiloxane (PDMS) microfluidic device. The flowing stream containing photosensitive initiator was exposed to ultraviolet light from an inverted microscope. Particles were rapidly polymerized in arrays and were collected in the device reservoir. As shown in Figure 1.11, the shape of the particles was

determined by mask patterns, i.e., triangular, square, cylindrical. By co-flowing two streams containing PEG-DA and rhodamine labelled PEG-DA, nonspherical Janus particles were demonstrated.¹⁹

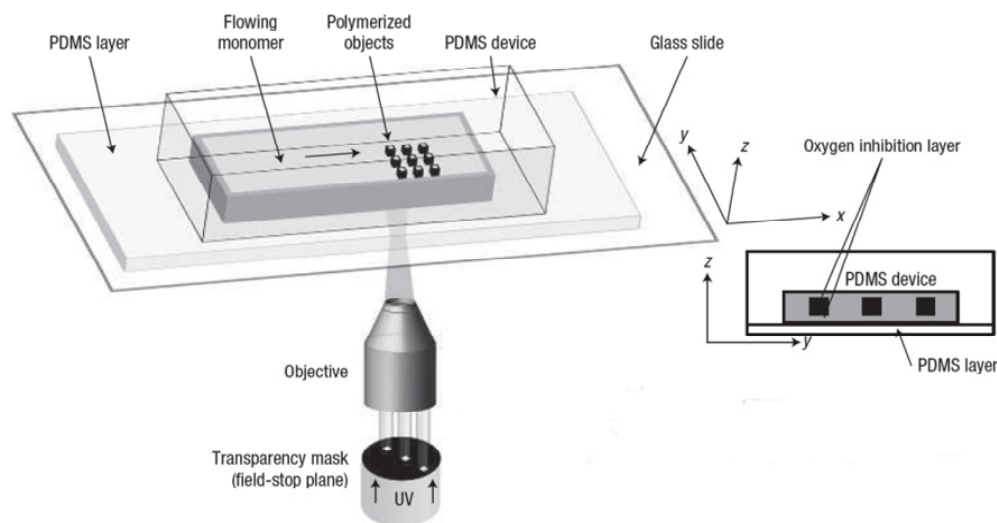


Figure 1.11 Continuous flow lithographic technique to produce Janus particles.¹⁹

1.6 Assembly of Anisotropic Colloids

Nonspherical building blocks have been predicted to assemble into a wide range of phases including nematic and smectic liquid crystals (Figure 1.12), rotator (or plastic) crystals and aperiodic (or degenerate) crystals.⁷

Figure 1.13A depicts the systematic phase behavior of nonspherical dimers between the limit of lobe fusion to a single sphere and the case of just-touching dimer lobes. As the system relative density increases, the diagram indicates a transition from the low density disordered phase into a plastic crystal (PC in Figure 1.13A) and traditional crystal (C in Figure 1.13A) at the highest density for the more isotropic shapes.⁸ Solidification to the degenerate crystal (Figure 1.13B) structure is predicted for highly anisotropic dimers with nearly tangent lobes. The degenerate crystal has distinct lobe-

based hexagonal order. However, the dimer orientations tile only the three crystallographic axes of the underlying triangular lattice. Shapes such as the pentamers in Figure 1.14 behave much like the highly lobe-fused dimers.⁶

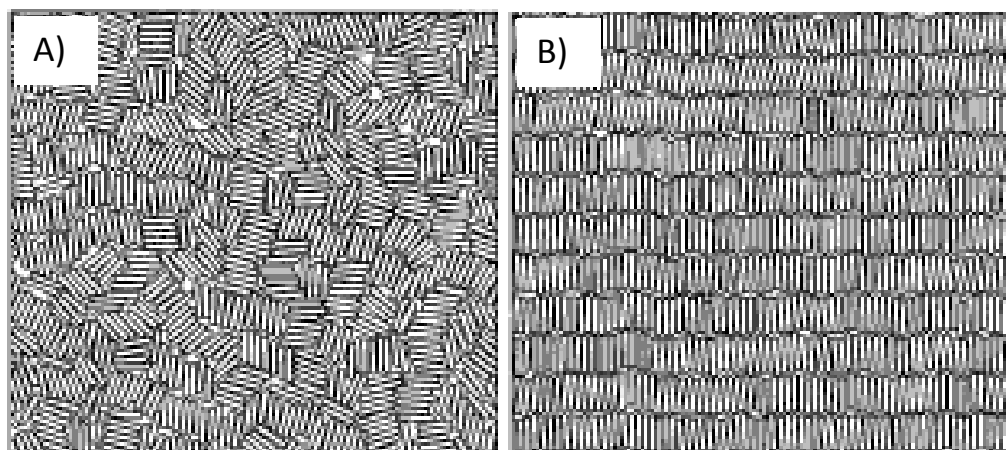


Figure 1.12 2D hard spherocylinders with a transition from an A) solid structure characterized by localized particle chaining to B) smectic liquid crystal phase.⁷

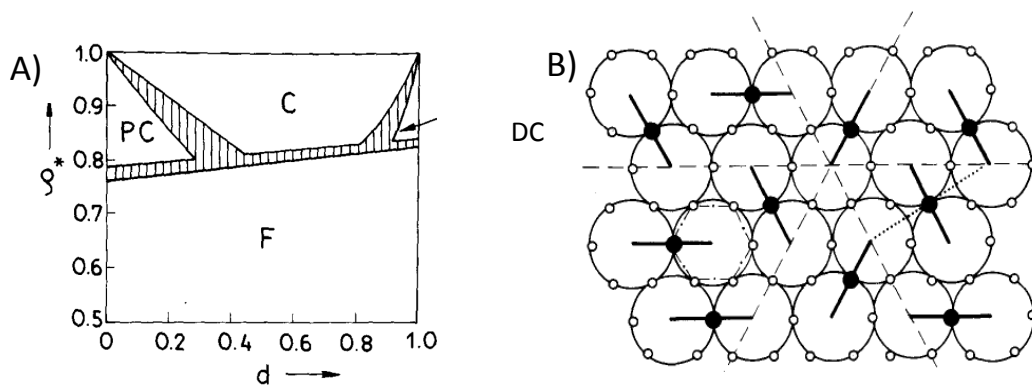


Figure 1.13 A) Phase diagram of dimer system. Shaded area indicates two phase regions for the first order phase transitions. d is the ratio of the center to center distance between the dimer and diameter of the dimer. q^* is the ratio of density and the close packing density. PC refers to perfect crystal, C refers to crystal, DC refers to degenerate crystals and F refers to the fluid phase B) Dimers in a close-packed degenerate crystal arrangement.⁶

Theoretical work (for example, Figure 1.14) has outpaced experiments due to challenges in obtaining order during real processing conditions. Issues such as gelation and jamming as well as shape and/or size polydispersity and particle-substrate interactions hinder self-organization. Experimental methods that have been shown to control particle crystallization include the convective and confinement assembly process.

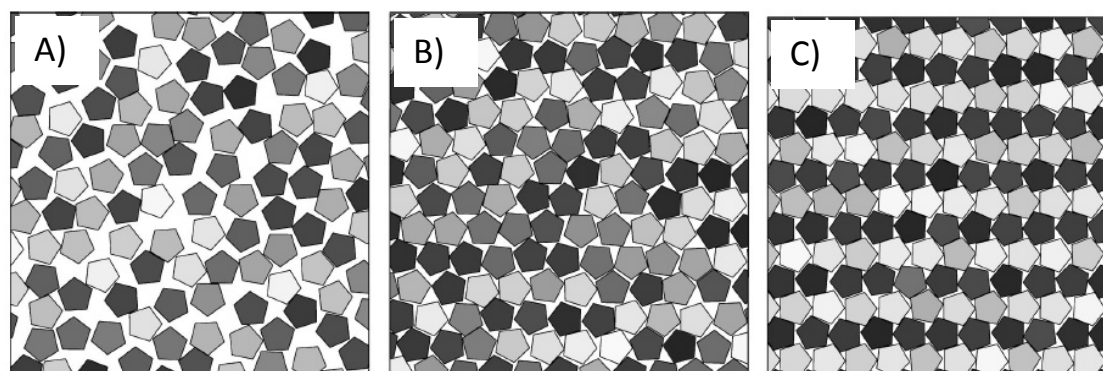


Figure 1.14 Simulation results for A) fluid, B) rotator and C) crystal phases formed by pentamer building blocks. Grey scale indicates similarly oriented pentamers.⁸

1.7 Convective Assembly of Colloidal Particles

Spherical colloidal particles self-assemble on a substrate at the drying front of a suspension when the dispersion medium (i.e., water) evaporates, as shown in the Figure 1.15. This technique is also known as convectively-assisted self-assembly or controlled drying.²⁰ The particle suspension concentration, evaporation rate, viscosity of the medium, particle size, substrate wetting properties, etc. influence the thickness and the quality of the crystals that are produced.

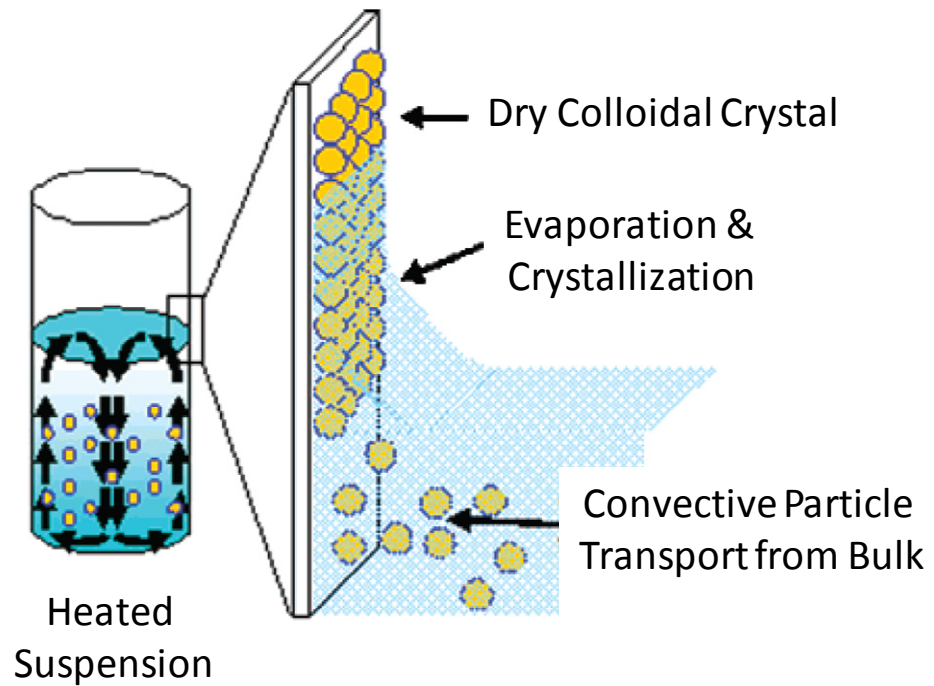


Figure 1.15 Convective assembly of spherical colloids.²⁰

1.8 Confinement Technique

Conventional microlithography can be used to construct fluidic cells. In a much less expensive embodiment of the device, a plastic gasket was sandwiched between two glass slides held together using binder clips. A hole drilled on the top glass substrate allowed injection of an aqueous dispersion of spherical colloidal particles. The glass slide was made hydrophilic to promote the assembly of long range ordered 3D arrays.²¹

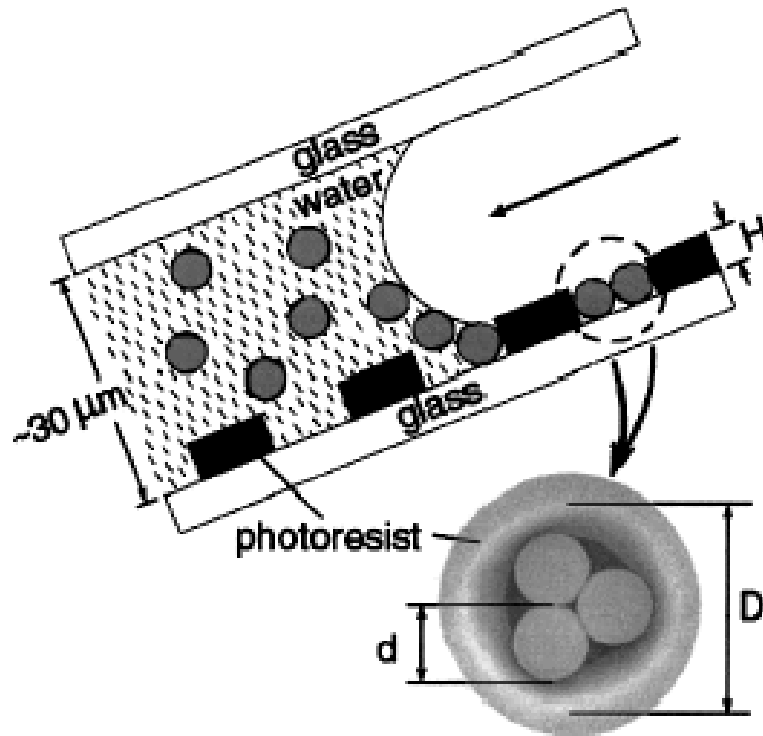


Figure 1.16 Confinement of colloidal particles and formation of uniform geometry clusters between two glass substrates of a fluidic cell.²¹

Pyramidal pits or V-grooves etched on the surface of Si (100) wafers have also been used as substrates in confinement cells. Polystyrene beads $\sim 1.0 \mu\text{m}$ in size were crystallized on patterned surfaces as shown in Figure 1.17. The square pyramidal pits forced the polymer beads to grow into 3D crystalline FCC structures with (100) planes parallel to the substrate surface.

Additionally, physical confinement has been employed to organize monodisperse spherical particles into uniform clusters. Cylindrical holes were patterned in a film of photoresist on the surface of the bottom glass substrate (Figure 1.16). Polymer beads were formed into polyhedral clusters inside the cylindrical holes as the particles were confined between glass slides.

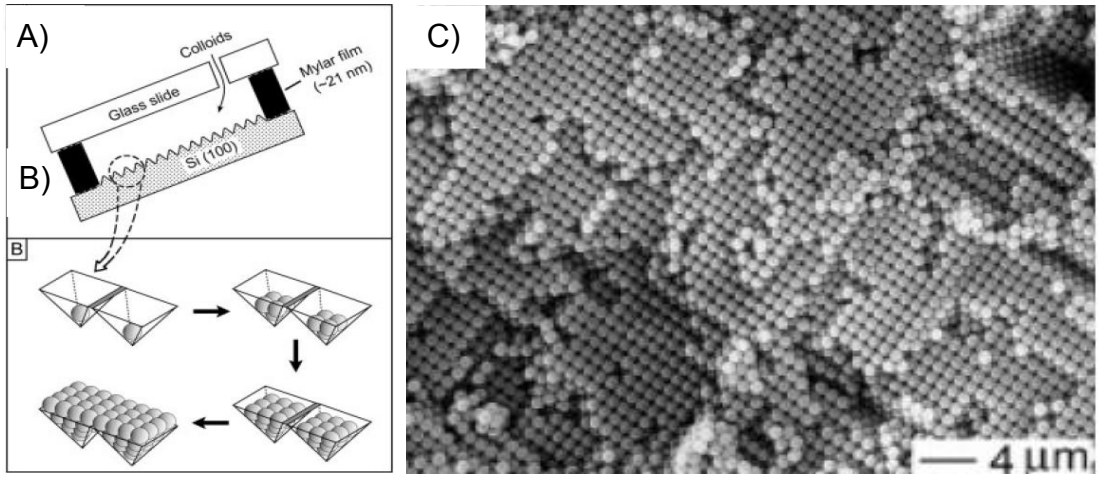


Figure 1.17 A) Confinement cell. B) Polystyrene beads packing in V-grooves of the substrate in A). C) FCC crystal with (100) lattice plane orientation as the top surface.²²

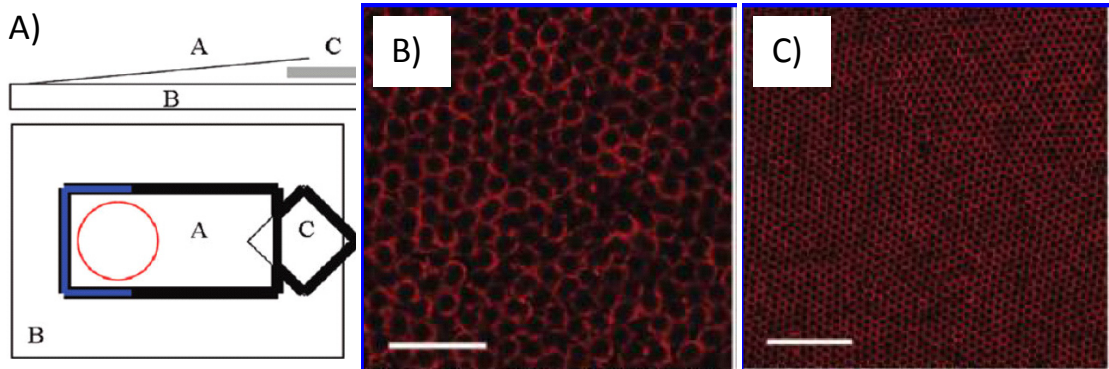


Figure 1.18 A) Wedge cell construction for confinement-assisted assembly of dimers. B) Rotator and C) hexagonal phase of dimers under confinement.²³

In an example of nonspherical confinement-assisted assembly, a suspension of silica-coated polystyrene dimers were confined between two glass slides propped up at an angle, using a small cover slip as shown in Figure 1.18.²³ The gradient in gap height allowed the particles to arrange into 2D planar phases along the incline.

Chapter 2

2 Results and Discussions

In this chapter, the synthesis and self-assembly of phases from uniform micron- and submicron anisotropic particles is described. Polymer colloidal particles with dimer and trimer shapes were prepared. The particles were organized using a confinement technique and the phases formed as a function of the gap-height in the containment system were examined using optical and confocal microscopy.

2.1 Synthesis of Linear Polystyrene Particles Using the Dispersion Polymerization Method

Standard dispersion polymerization²⁴ was used to synthesize monodisperse linear polystyrene (LPS) particles as seeds for further procedures. Monomer seed droplets were stabilized in a mixture of ethanol and water medium by sodium lauryl sulfate, used as an emulsifier. The surfactant forms a micelle with its hydrophobic end on the interior and the hydrophilic end towards the surface. In order to reduce surface tension, the micelle assumes a spherical shape and continues to grow as more monomer enters. The micelle stops growing when the monomer present in the ethanol/water mixture is consumed. Polymerization is initiated by potassium persulfate that generates free radicals. Linear polystyrene (LPS) particles of 430-470 nm diameter were synthesized (Figure 2.1A).

2.2 Synthesis of Crosslinked Polystyrene Particles Using a Seeded Emulsion Polymerization Technique

Subsequent swelling of the LPS with monomer, crosslinker and initiator for 24h followed by free radical polymerization at an elevated temperature (70°C) leads to the

formation of crosslinked polystyrene (CLPS) particles. The crosslinking density of the polymer chains inside the CLPS was varied by manipulating the amount of divinylbenzene (DVB, 55% isomer) during the swelling step.^{15,25} Highly crosslinked (25-30% DVB) spherical CLPS of approximately 700-750nm in diameter as shown in Figure 2.1B were synthesized.

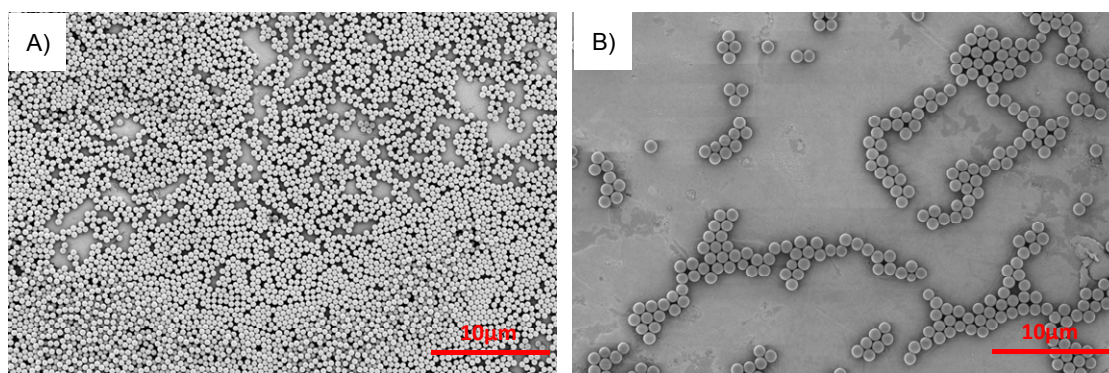


Figure 2.1 A) Linear polystyrene and B) crosslinked polystyrene particles.

2.3 Synthesis of Anisotropic Dimer -Shaped Particles by Protrusion of Daughter Lobe from CLPS

Previous studies have demonstrated that the dynamic swelling method²⁶ (DSM) for adsorbing monomer onto a crosslinked polymer particle leads to the formation of a secondary lobe. Monomer dispersed in an ethanol/water mixture phase is separated into small droplets and adsorbed by the crosslinked particle as water is introduced to the system dropwise. The monomer phase continues to grow as more water is added. In the schematic model shown in Figure 2.2, a variety of degrees of monomer adsorption on a polymer particle are shown. The phase in which monomer is completely separated from the crosslinked polymer particle has contact angle θ_p of 0° and volume percentage of the polymer engulfed by the monomer phase, V_{eng} of 0%. For intermediate ‘snowman’

shaped states, θ_p is between 0° and 180° and V_{eng} is between 0 and 100%. For the core-shell shape, the angle is 180° and V_{eng} is 100%.

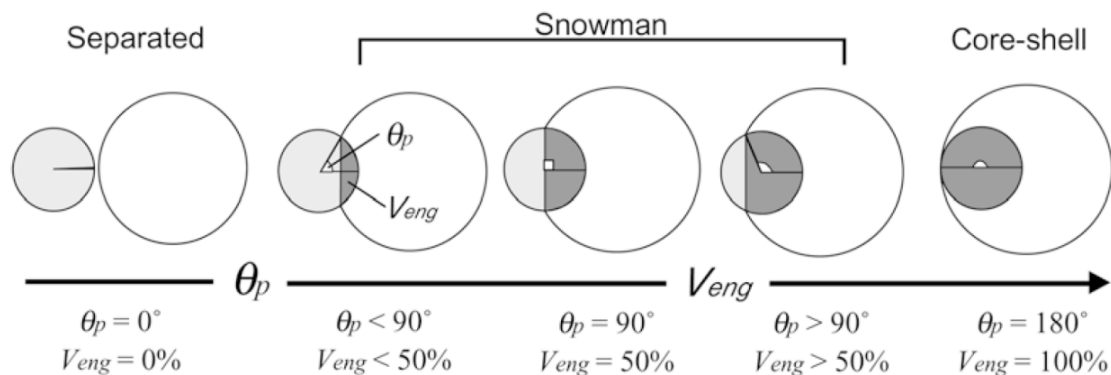


Figure 2.2 Schematic of monomer droplet adsorbed onto the crosslinked particle compelling lobe interpenetration by the ‘dynamic swelling method’.²⁶

Another report describes coating CLPS particles with a grafted layer of polyacrylic acid (PAA) prior to swelling.¹³ As the coated particles are swollen with monomer and initiator, the polymer chains inside the seeds stretch from their relaxed equilibrium configuration. Raising the temperature allows the chains within the seed particles to recoil and the seed particle contracts, driving out the monomer. Due to the presence of hydrophilic coating on the polymer surface, the expelled droplet of monomer forms a bulge rather than a uniform coating on the surface of the seed. The degree of separation of the monomer droplet from the seed depends on the interfacial tensions of the polymer and aqueous phase, $\gamma_{P,A}$, the monomer and aqueous phase, $\gamma_{M,A}$, and the polymer and monomer phase. Rearranging the analog to Young’s equation for a liquid droplet on a solid surface in the presence of vapor gives,

$$\cos\theta = \frac{\gamma_{P,A} - \gamma_{P,M}}{\gamma_{M,A}}$$

where θ is the contact angle between the monomer and the seed particle. As the difference between $\gamma_{P,A}$ and $\gamma_{P,M}$ decreases, the contact angle increases and the bulge becomes more distinct. As shown in Figure 2.3, when surface wetting becomes completely unfavorable, the monomer forms a separate droplet outside the seed particle (as in Figure 2.3D) and in the case of complete wetting the monomer coats the surface of the seed uniformly (Figure 2.3A). The intermediate geometries depend on the interfacial tension between the monomer and the bulk in the presence of the coating.

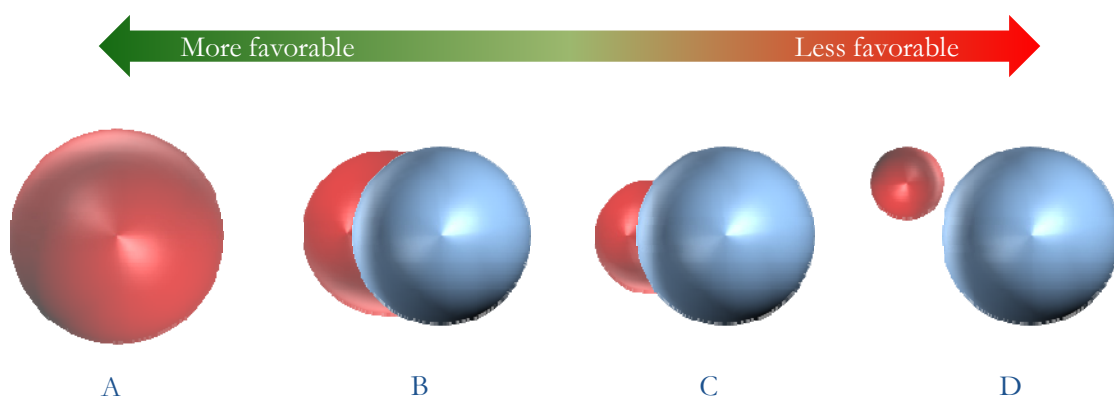


Figure 2.3 Schematic showing states of expulsion of monomer from CLPS A) complete wetting B) moderate wetting C) mild wetting D) zero wetting.¹³

2.4 Synthesis of Trimer Shaped Particles from Parent Dimer Particles

Rod or triangular-shaped particles have been synthesized by performing seeded polymerization on dimers (Figure 2.4).¹² Tailoring the crosslinking density gradient between the two lobes of the dimers gives rise to systematic tuning of the shape characteristics. For example, dimers that contain lobes with different crosslinking density become rods when swollen and polymerized. Dimers with two lobes having equal crosslinking density become triangular. The gradient in crosslinking density is tuned by adjusting the relative concentration of DVB during the swelling step to form each lobe.

Between the two critical values of density gradient that lead to either rods or triangular shapes, batches with a mixture of both trimer particle morphologies can be obtained. The crosslinking density was linked to the difference in viscosity in the swollen dimers. In case of the triangular particles, the viscosity inside the swollen dimers is high due to the more substantially crosslinked network in both lobes. Hence, it is more difficult for the monomer to flow throughout the existing lobes of the dimer — i.e., 3h for triangles versus 38s for rods to form a third lobe in kinetic studies. By tuning the synthesis conditions, the particles in a particular batch obtained were of one type (i.e., either pseudo-linear or triangular by perpendicular lobe growth).

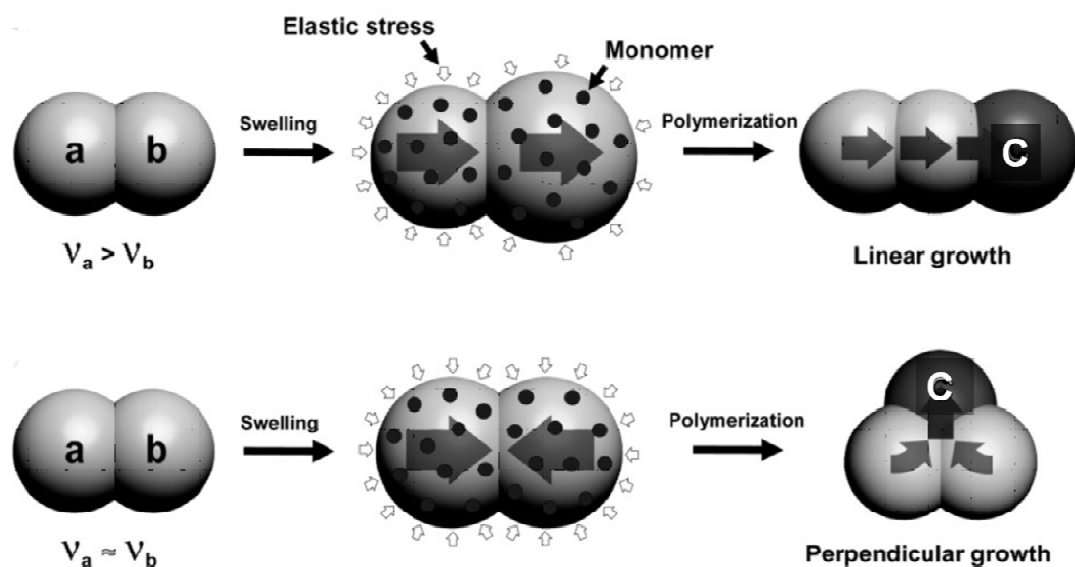


Figure 2.4 Schematic protrusion of third lobe from dimers in line with the parent lobes to produce A) straight particles (linear growth) and B) bent morphology perpendicular to the parent lobes (perpendicular growth). Values v_a and v_b represent the degree of crosslinking of lobe a and lobe b, respectively.¹⁶

The principles described by Weitz et al.¹⁶ produce particles in the size range of 5-10 μm . To synthesize trimer particles in the micron/submicron length scales the surface tension of the particle needs to be manipulated. Since the surface area of particles in this size range is large, the interfacial effects may dominate the forces generated by elastic stress and prevent the expulsion of a lobe. Anisotropic particles in the micron to submicron size range are important building blocks because they have considerable stability against settling in dispersion media and show greater ability to sample configurations via Brownian motion or thermal agitation. Additionally, structures made from submicron to micron sized colloids have the ability to control light waves in the visible and near-IR regions and thus are desirable as building blocks for fabricating photonic crystals.

Here, trimers in the size range of 1-2 μm were synthesized using dimers as seeds. Figure 2.5 details the synthesis parameters under which experiments were carried out. Scheme A describes the synthesis of trimers from two dimer shapes (shown in Figure 2.6C and 2.6D). Both dimer seeds were coated with acrylic acid (AA) to have hydrophilic coating density of $\sigma = 2$ [i.e., $\sigma = 2 \times 10^{-21}$ g/nm²], swelled with a ratio of 3:1 (monomer: polymer concentration ratio) and 5% DVB for 24 h and then polymerized. In addition as another comparison, the seeds shown in Figure 2.6C were swelled at a ratio of 3:1 with hydrophilic coating density ($\sigma = 0, 2, \text{ and } 4$) as outlined in Figure 2.5 (Scheme B). Trimers were also formed at swelling ratios 2:1, 3:1, 4:1 and 5:1 from dimers with a hydrophilic density of $\sigma = 2$, keeping all other conditions the same.

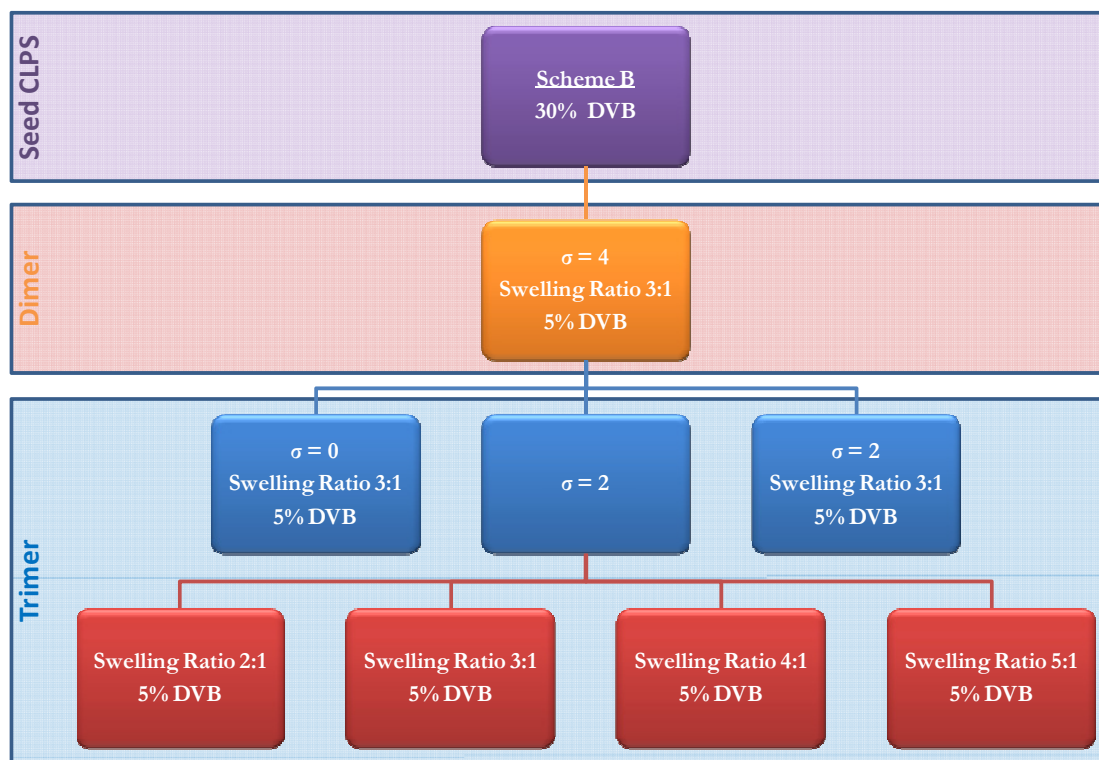
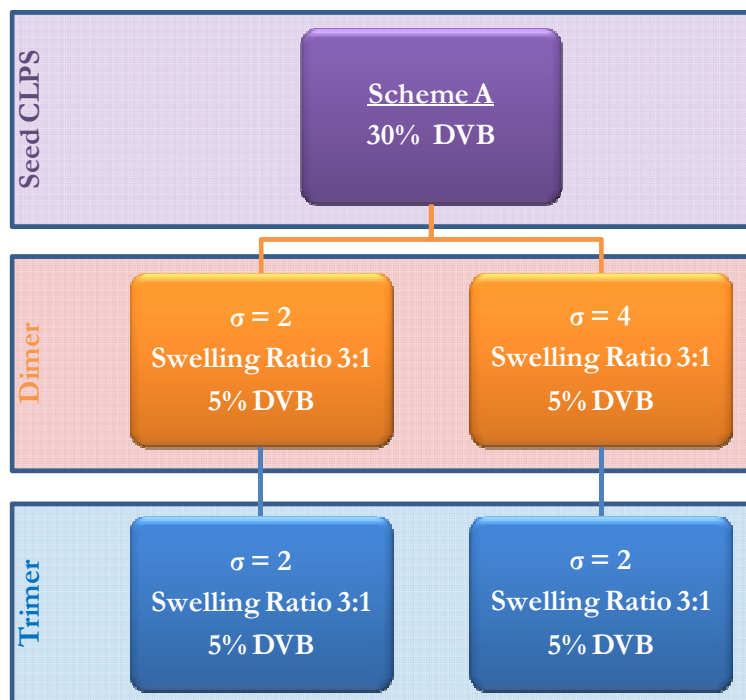


Figure 2.5 Experimental schemes for synthesis of trimers.

The CLPS with 25% DVB, coated with hydrophilic density of $\sigma = 4$ produced dimers shown in Figure 2.6A, and dimers shown in Figure 2.6B when treated with a hydrophilic coating density of $\sigma = 2$. CLPS with 30% DVB produced dimers in Figure 2.6C and 2.6D when coated with a hydrophilic coating density of $\sigma = 4$ and $\sigma = 2$, respectively. For a given swelling ratio and crosslinking density, as the surface wetting becomes energetically unfavorable (σ increases) the phase separation becomes more distinct, as indicated by the center-to-center distance between lobes. This trend is clearly shown for the dimers in Figure 2.6.

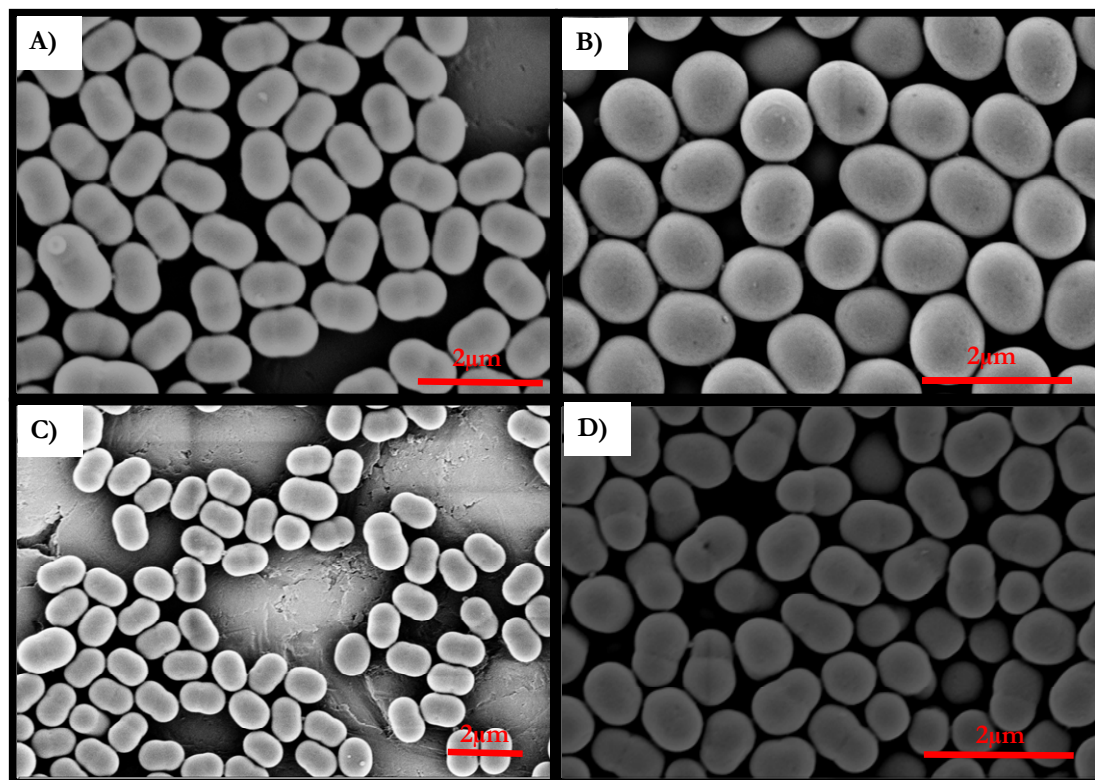


Figure 2.6 Dimers synthesized from CLPS A) 25% DVB $\sigma = 4$, B) 25% DVB $\sigma = 2$, C) 30% DVB $\sigma = 4$ and D) 30% DVB $\sigma = 2$.

Additionally, a lower degree of lobe fusion and higher lobe asymmetry is apparent in the dimers of Figure 2.6D (30% DVB, $\sigma = 2, 3:1$) as compared to those in Figure 2.6B (25% DVB, $\sigma = 2, 3:1$). The crosslinking density of the seed influenced the morphology of the final dimer in that a lower crosslinking density (25%) produced a more symmetric, spherocylindrical or ‘egg’ shape. Particles with higher crosslinking density (30%) show a greater tendency to form a bulge that grows so that the seed becomes well-distinguished from the expelled monomer phase. This is consistent with the rationale that a denser network of crosslinking generates more elastic driving force for separating the polymer chains from the encapsulated monomer.

Figure 2.7 demonstrates the effect of swelling ratio on the shape of the trimers. Dimers swollen with 2:1 swelling ratio phase separated a daughter lobe that was small and not distinct. The 3:1 ratio produced a well-separated third lobe comparable in size to the lobes of the parent dimer. A bidisperse population consisting of straight and angular particles was observed (as shown in Figure 2.7B-D). Swelling the seeds at a ratio of 4:1 resulted in a third lobe that had a larger diameter than the lobes of the parent dimer, as shown in Figure 2.7E-G. This greater swelling ratio made more monomer available for formation of the third lobe. Similar to the 3:1 case, straight and angular trimers were produced. Though the large lobe continues to grow in size at a swelling ratio of 5:1, the sample becomes polydisperse, as a fourth protrusion with a range of sizes occurs. The tendency to expel two lobes in one process step was clearly due to availability of excess monomer when the higher swelling ratio was applied. Figure 2.8 provides the plot of third lobe diameter as a function of swelling ratio.

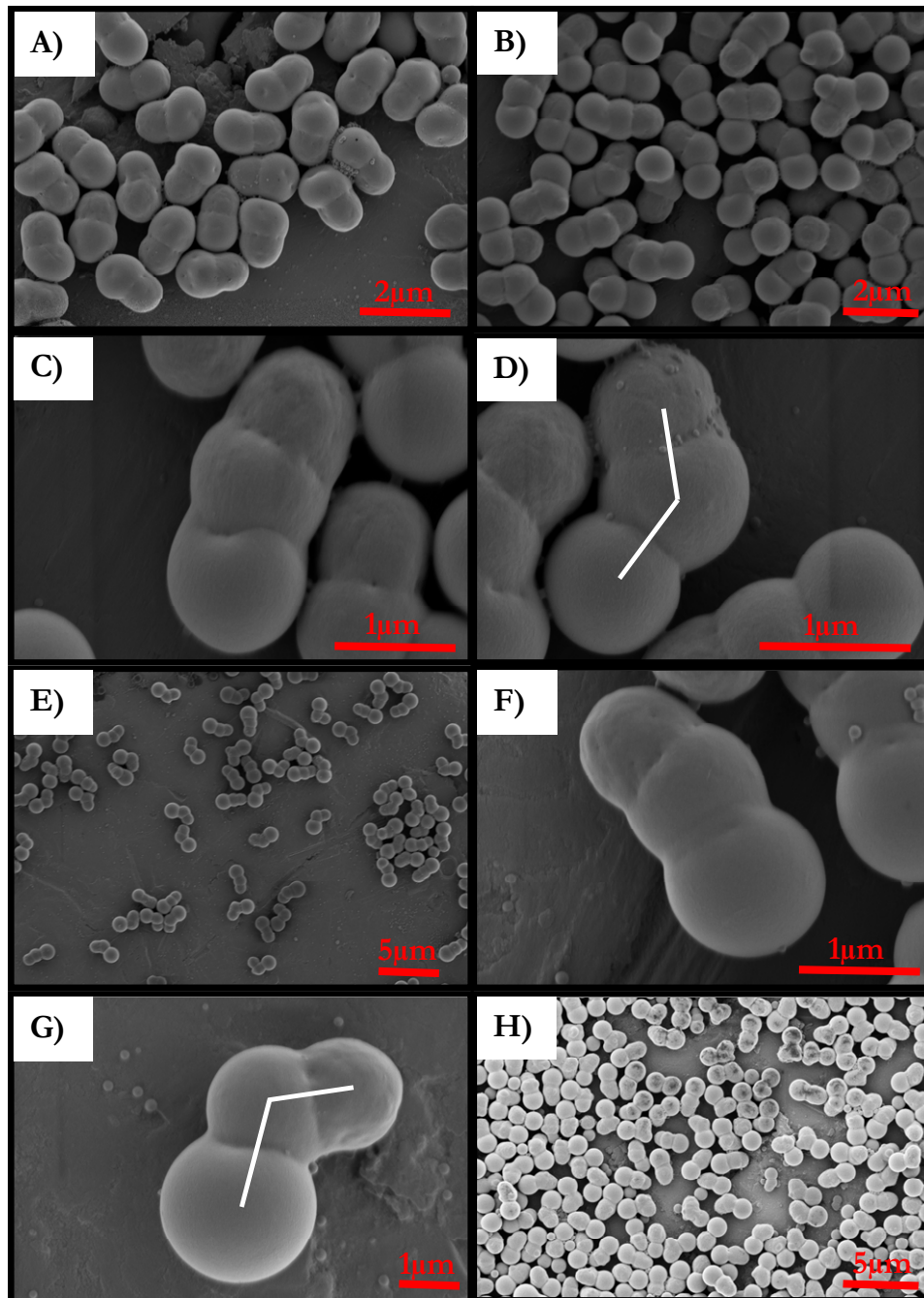


Figure 2.7 Trimers synthesized with a swelling ratio of A) 2:1, B) 3:1, C) 3:1 (straight trimer, enlarged view), D) 3:1 (angular trimer, enlarged view), E) 4:1, F) 4:1 (straight trimer, enlarged view), G) 4:1 (angular trimer, enlarged view) and F) 5:1. White lines show the center-to-center distances. For ‘bent’ trimers the angle between segments that connect adjacent lobes was roughly 110° - 135° .

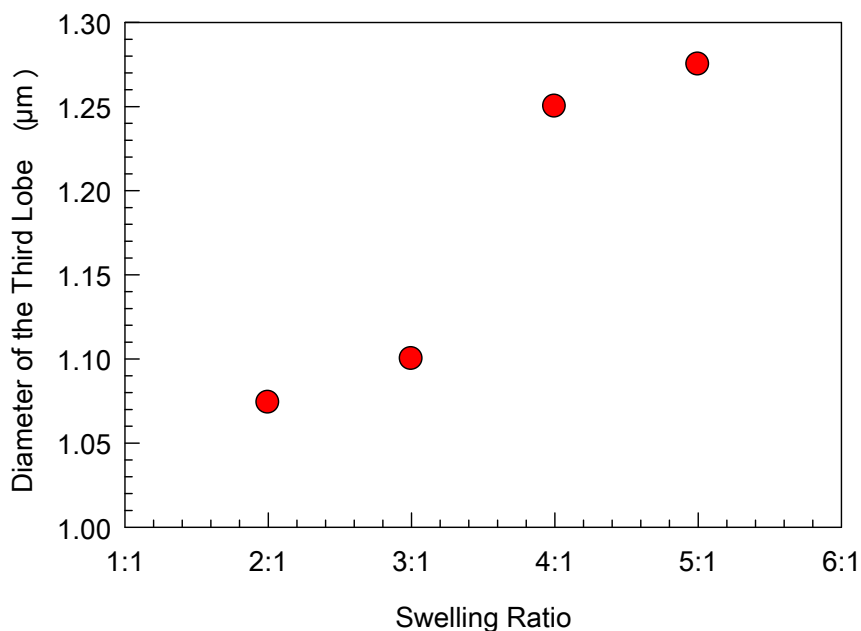


Figure 2.8 Plot showing increase in the third lobe diameter with monomer to polymer swelling ratio.

In the absence of AA coating on the seed particles ($\sigma = 0$) prior to swelling (3:1) and polymerization, the trimers in Figure 2.9A were produced from the dimers shown in Figure 2.6C (30% DVB, $\sigma = 4$). The resulting lobes were not well-separated from the seed dimers, since there was little dewetting. In contrast, the distinctly segmented trimers in Figure 2.9B were obtained from the more asymmetric dimers in Figure 2.6D (30% DVB, $\sigma = 2$), after coating the seeds at a density of $\sigma = 2$ and swelling (3:1).

Trimers in Figure 2.7B and 2.9B were synthesized from seed dimers in Figure 2.6C (30% DVB, $\sigma = 4$) and dimers in Figure 2.6D (30% DVB, $\sigma = 2$), respectively, after coating the seeds with hydrophilic coating density of $\sigma = 2$ and swelling with 3:1 monomer to polymer concentration ratio. In the case of trimers shown in Figure 2.7B, a bidisperse population of straight and angular particles was observed with three well-

separated lobes, whereas in the case of trimers in Figure 2.9B the particles were fairly uniform and nearly straight with a middle lobe that remains largely engulfed. The amount of surface modification at the initial stage of dimer formation seems to influence the level of wetting when the monomer phase separates from the dimer seeds producing trimers. The dimer shape as well is altered for the two conditions of hydrophilic coating density and this may also cause a smaller degree of dewetting for the trimer third lobes in Figure 2.9B. From our experiments, we deduce that both hydrophilic coating density and crosslinking density gradient play a key role in determining the final shape and uniformity of the trimers.

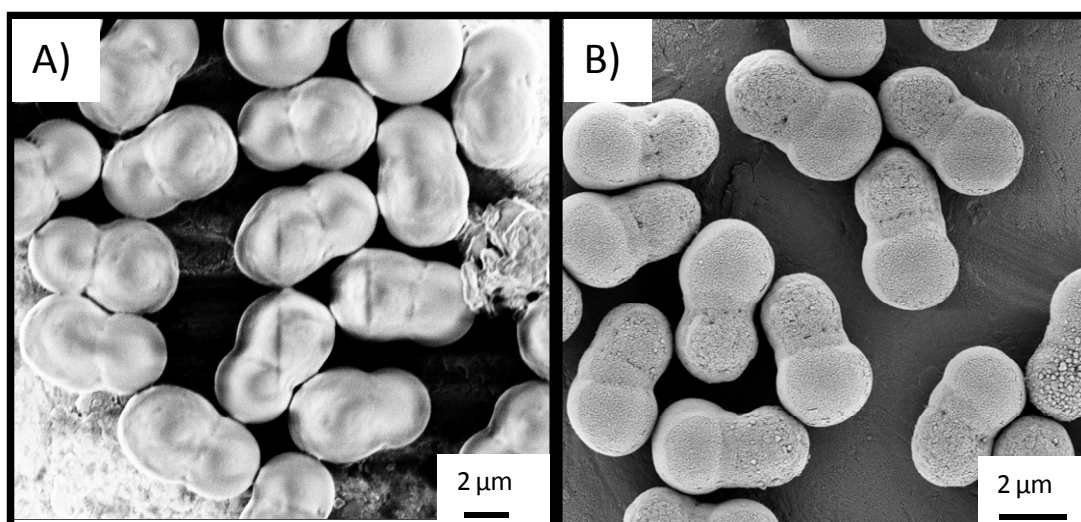


Figure 2.9 Trimers synthesized from A) dimer seed particles (30% DVB, $\sigma=4$) with coating density, $\sigma=0$ and B) dimer seed particles (30% DVB, $\sigma=2$) with coating density $\sigma=2$.

Prior reports that produce schematics such as Figure 2.4 do not account for the surface tension effects considered here. With the large difference in crosslinking density between the dimer lobes expected from CLPS (25-30% DVB) and 5% DVB second stage

protrusion, a linear trimer should be favored. However, reproducible angles for the bent trimers suggest that new ‘bond-angle’ values are stable between those generated by the extrusion of a lobe either parallel (Figure 2.4, top) or perpendicular (Figure 2.4, bottom) to the seed dimer major axis. The bond angle parameter depends also on the relative sizes of the lobes. Values near 105° provide a colloidal means to ‘synthetic water molecule’ shapes.¹⁸

2.5 Silica Coating of Dimer and Trimer Polystyrene Building Block

The dimer and trimer shaped PS colloids were coated with rhodamine isothiocyanite (Figure 2.10A) labeled silica shells to render the particles suitable for imaging by confocal microscopy (Figure 2.11).²⁷ The shell formation on the polymer template is promoted by the adsorption of 3-aminopropyltriethoxysilane (Figure 2.10B), a coupling agent. From the dimensions of the particles calculated after coating, L^* and $1-s^*$ for the coated dimers (Figure 2.12) were found to be 0.7 and 0.13 (Table 2.1). The corresponding values for the trimers were 0.83 and 0.17. L^* refers to the degree of fusion of the daughter lobe with the parent lobe and is defined as the ratio of the center-to-center distance between the two lobes (L) and the diameter (D_L) of the large lobe. The s^* term refers to the symmetry of the dimer and is defined as the ratio of the diameter of the two lobes ($s^* = D_S/D_L$). A large L^* value indicates well-separated lobes and $1-s^*$ values approaching zero refer to colloids that are nearly spherical in shape.

Table 2.1 Shape parameters of nonspherical polystyrene particles.

Particle Type	L^*	s^*	$1 - s^*$
dimer	0.67	1.00	0.00
silica-coated dimer	0.70	0.87	0.13
silica-coated trimer	0.83	0.83	0.17

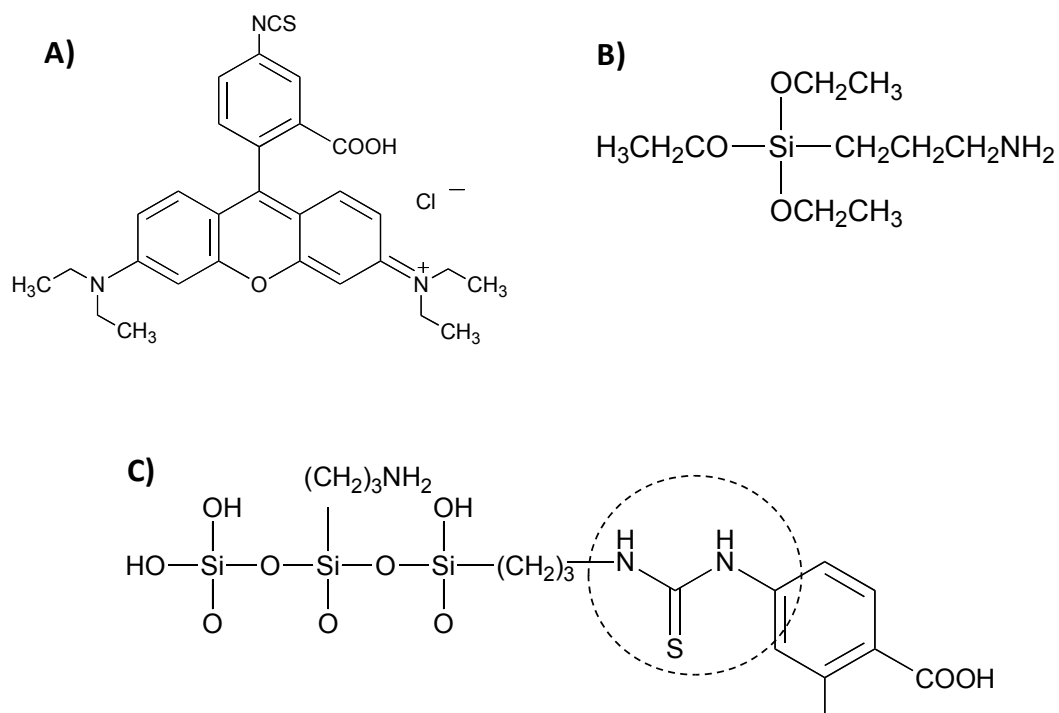


Figure 2.10 A) Rhodamine isothiocyanate (RITC), B) 3-aminopropyltriethoxysilane (APS), and C) APS-RITC complex. Circled region in C) shows linkage of the two molecules.

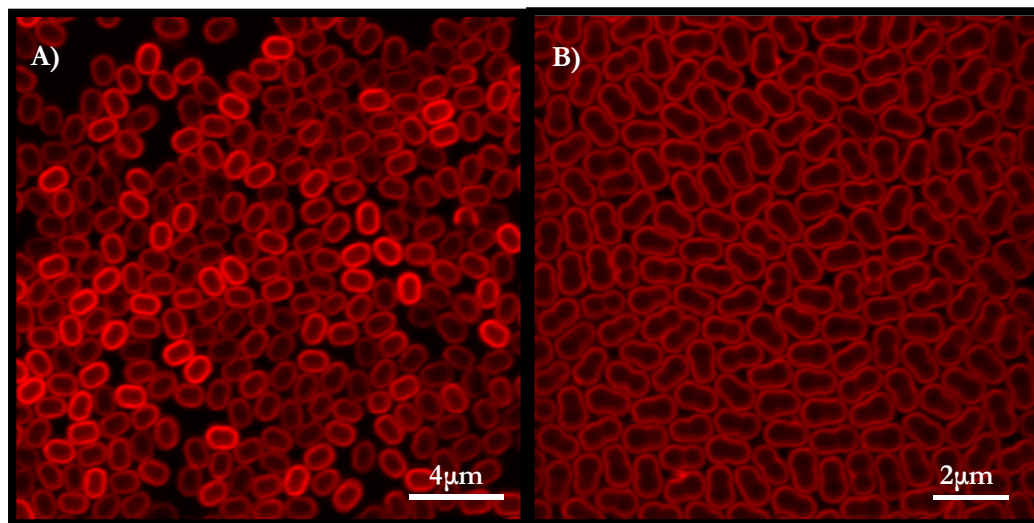


Figure 2.11 Fluorescence micrographs of A) silica coated dimers and B) silica coated trimers.

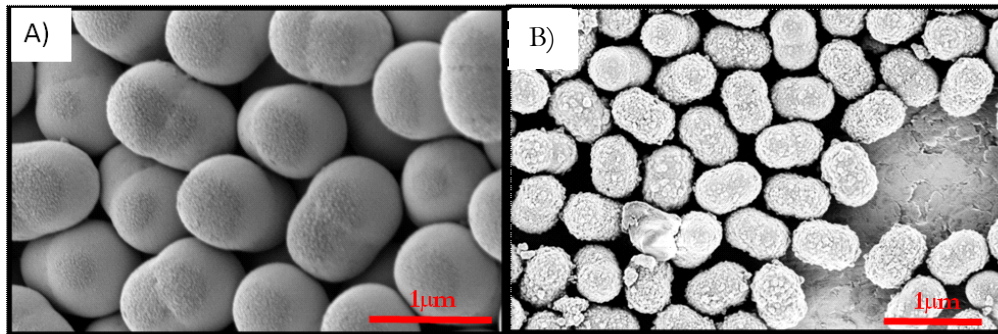


Figure 2.12 A) Bare and B) silica coated dimer building blocks for assembly.

2.6 Self-assembly Under Confinement

Studies on the self-assembly of trimeric proteins provide a motivation for investigating assembly of trimer-shaped colloidal particles. Protein molecules can arrange themselves into 2D and 3D crystal structures, particularly when bound to the surface of a membrane. Monte Carlo simulations (Figure 2.13) were used to theoretically study the structure and phase behavior of trimer proteins. The trimeric molecules were modeled as triangular hard discs.²⁸ Attractive interactions introduced by functionalizing one disc of the trimeric unit were considered. An example of the trimeric protein, Annexin A5, that was reported to self-assemble on the surface of phospholipids into p6 and p3 crystal structures is provided in Figure 2.14.²⁹

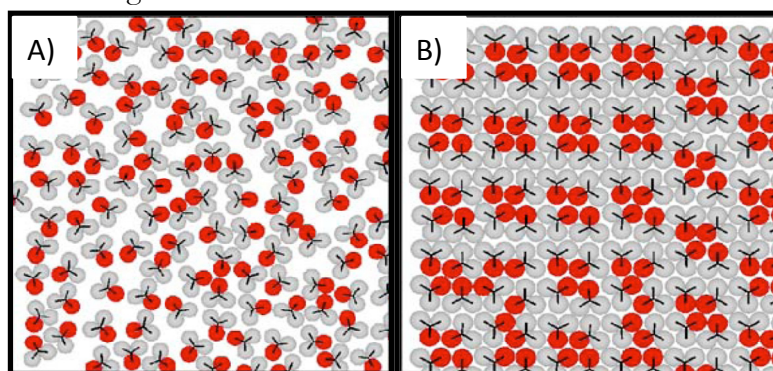


Figure 2.13 Monte Carlo (MC) simulation for self-assembly of trimer building blocks with functional lobe. A) Low density fluid phase and B) high density ordered structure of trimers.²⁸

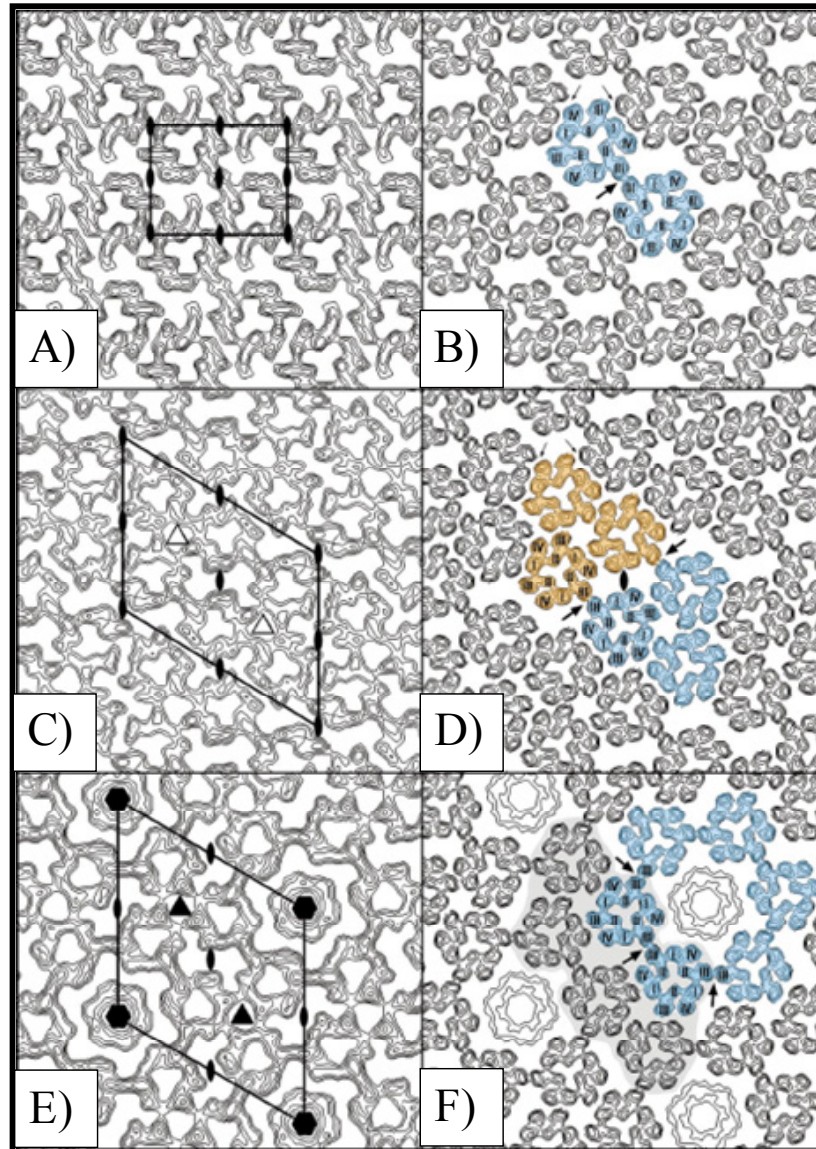


Figure 2.14 A, B) 2D projection map of crystal form 1 ($c2mm$ plane group). The lattice points correspond to dimer units composed of Annexin A5 trimers. The crystal form is rectangular. A dimer unit is highlighted in blue. C, D) 2D projection map of crystal form 2 ($p3$ plane group). The repeat unit consists of two groups of three Annexin A5 trimer. The two groups are highlighted in blue and orange. E, F) 2D projection map of crystal form 3 ($p6$ plane group). The motif is made of six trimers arranged at the vertices of a hexagon which is highlighted in blue. The hexagonal unit surrounds a central disordered trimer.²⁹

Structural ordering and phase transitions of colloidal crystals can be influenced and studied by confining suspensions within small angled wedges of two flat glass plates. Along with crystalline structures, systems of non-spherical particles can be captured in liquid crystal and other molecular solid phases. For instance, the plastic crystal (rotator) state refers to molecules arranged on an ordered lattice, but having orientations that are random.³⁰

A prior study on self-assembly of asymmetric dimers (Figure 2.15) under physical confinement in a wedge cell showed a range of phases as a function of the confinement height. Towards the bottom of the cell where the gap height is comparable to the lobe diameter, the particles are oriented in-plane forming a monolayer. Along the wedge, as the gap height increased and the particles had more room to tumble, they created a quasi-2D rotator phase. With further increase in gap height, the particles are sufficiently spaced to completely re-orient with their long axis out-of-plane in the monolayer phase. The particles in this region ultimately densely pack and crystallize into an ordered hexagonal arrangement. Beyond the monolayer phase heights are bilayered structures and subsequent multilayered phases which may be disordered.²³

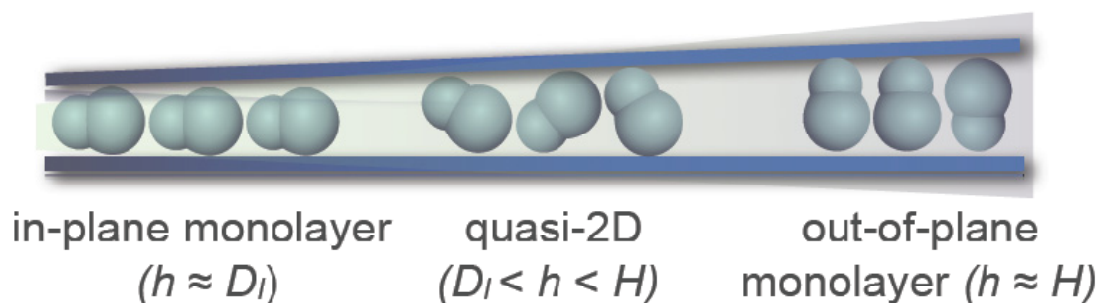


Figure 2.15 Wedge cell constructions for asymmetric dimers showing variation of particle orientation and ordering with gradient in height.²³

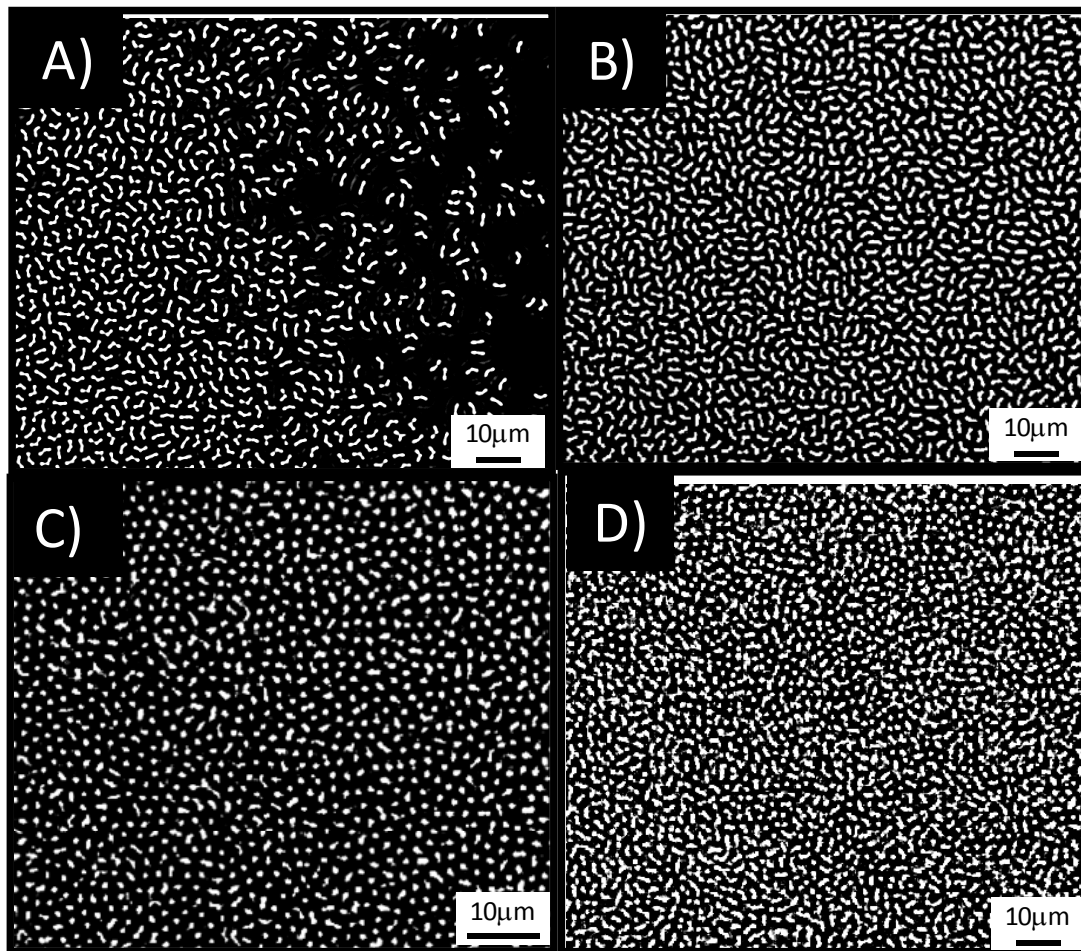


Figure 2.16 Optical micrograph of A) edge of in-plane monolayer phase, B) high density monolayer phase, C) out-of-plane monolayer phase and D) multilayered phase.

In the current study, the phases formed by ‘water-molecule’ shaped trimers (Figure 2.7B) confined between two glass slides in a wedge cell were observed. Towards the narrow region of the cell where the gap height is similar to the film thickness of the in-plane monolayer, the particles were lying flat on the surface of the substrate as shown in Figure 2.16A. The particles gradually became more densely packed as shown in Figure 2.16B. This phase shows local regions of particle chaining. The particles began to reorient to the out-of-plane monolayer alignment as the gap height increased. This phase had local rhombic and hexagonal regions of packing, but displayed no long range order

(Figure 2.16C). Polydispersity arising from minor variations in trimer bond angle, lobe size or from a second population of straight trimers may disrupt the quality of ordering. Also, occasional adhesion of particles to the glass surface can inhibit the ability to rearrange into close-packed ordered configurations. The out-of-plane monolayer phase was followed by a multilayered phase where the particles were highly disordered (Figure 2.16D) in the dense solid phase. Both in-plane and out-of-plane projections are apparent in the image.

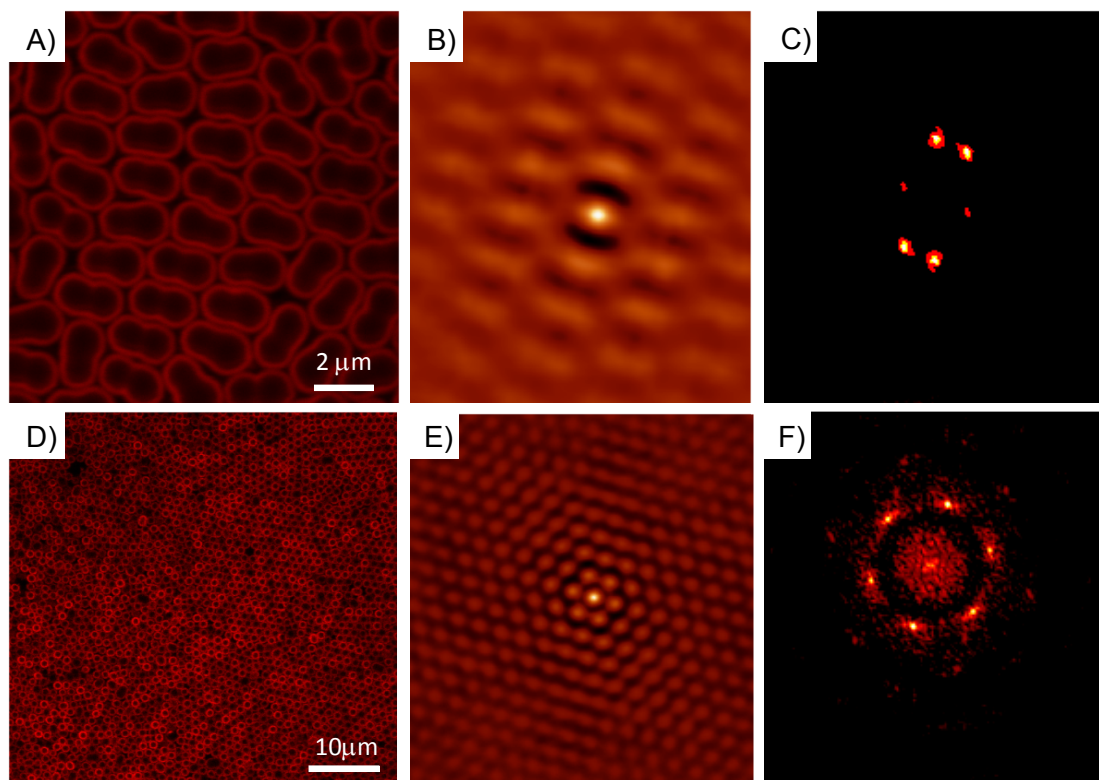


Figure 2.17 A) Confocal images of in-plane monolayer. B) Probability density of finding an aligned particle at a given displacement in-plane monolayer phase. C) FFT of in-plane monolayer. D) Confocal micrograph of trimers oriented out-of-plane. E) Probability of finding an aligned particle at a given displacement of out-of-plane oriented trimers. F) FFT of out-of-plane monolayer.

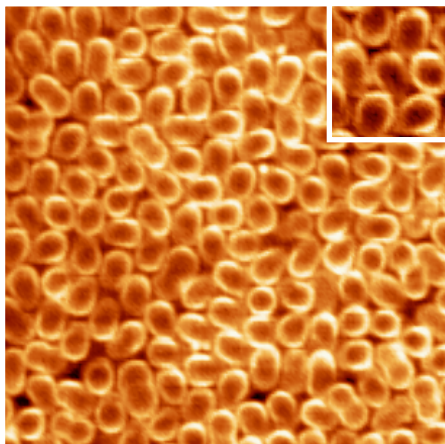


Figure 2.18 Intermediate phase for z-height between that of the in-plane and out-of-plane oriented structures for silica-coated trimers (2.12B). Inset shows an enlarged view.

As well, the phases formed by the silica-coated trimer building blocks of Figure 2.12B were examined in a confinement cell. Two of the phases that evolved as a function of increasing gap height and were observed using the confocal microscope are shown in Figure 2.17A, D. At the lowest part of the cell where the gap height is small, an in-plane monolayer occurred. There was no long range order, but small oblique grains could be found. FFT spot patterns and autocorrelations for the in-plane phase indicate the oblique symmetry.²⁰ As in the dimer studies referenced, Figure 2.17E, F show FFT spot patterns and autocorrelations for the out-of-plane monolayer phase of trimers (Figure 2.17A) with six-fold hexagonal symmetry. Between the in-plane and out-of-plane oriented regions, an interesting quasi-2D structure of the trimers was observed as shown in Figure 2.18. The trimers in this intermediate height region were tilted at acute angles with respect to the substrate. Rather than the tumbling motion of shorter dimers, the trimers exhibit conical gyration about a central positional axis. The bent shape of the trimer may provide enhanced stability for these orientations of the particle major-axes. The positional order within grains is roughly on an oblique lattice (distorted hexagonal packing).

Chapter 3

3 Summary and Future Directions

We have utilized a method to synthesize dimer and trimer colloidal particles of different symmetries, shapes and sizes. Crosslinking density, hydrophilic coating density and swelling ratio may be carefully tuned to obtain uniform particles of a range of shapes and sizes using seeded emulsion polymerization. Studies in future directions may involve preparation of a wider variety of particles with shape anisotropy tailored for photonic crystals.^{14, 15, 26, 31, 32}

New ‘bent’ trimer colloids were obtained using the seeded emulsion polymerization method with surface modified hydrophilic dimers. The quality of crystals produced by self-assembling these building blocks will be improved as more monodisperse populations of angular trimers are synthesized.

Greater shape monodispersity in the trimers may be realized by modifying the dimers with an even higher surface density of hydrophilic groups ($\sigma = 4$) in the third polymerization stage. The excess coating may help to more consistently direct the protrusion of lobes to the obtuse ‘bond angle’ condition by increasing the surface tension. Additionally, the particle surfaces can be further treated with polyvinylpyrrolidone (PVP) to prevent the adhesion to the glass surface that disrupts the self-assembly process. The thickness of the silica coating and the dye incorporation amount can also be optimized to decrease uncontrolled aggregation with the substrate.^{22, 33}

Additionally, dimers and trimers with functionalized lobes will be synthesized and used to study the effect on self-assembly of chemical anisotropy combined with shape anisotropy. Chemical anisotropy will be introduced in the daughter lobe of the dimer by swelling with monomer such as glycidylmethacrylate, vinylsilane, or 9-vinylanthracene.¹² Specific interparticle interactions can be further designed by incorporating iron nanoparticles as the seed in surfactant free emulsion polymerization synthesis. This seed can then be used for making dimers with one pure polystyrene lobe protrusion. The route introduces magnetic functionality to the trimer prepared from the Fe-PS composite dimer.³⁴⁻³⁷

To form high refractive index contrast porous structures, PS cores can be etched out by heat or plasma treatment after cell drying and infiltration of inorganics such as Si, Ge, HfO₂, TiO₂, etc. As well, multilayered structures can be produced to form 3D crystals. Measurements on the 3D crystals using normal incidence reflection spectroscopy may allow us to correlate structure with optical stop bands and band gaps. These can be compared to photonic band calculations to explore the role of symmetry at lattice sites in controlling dispersion relations and creating strong light-matter interactions.

APPENDIX

Experimental: Particle Synthesis

Non-spherical polystyrene (PS) particles were prepared using a seeded emulsion polymerization technique. Non-crosslinked monodisperse PS spheres with diameter 450 nm were synthesized. 1 g of PS spheres was swollen with 3 mL styrene monomer and 30 volume % of divinylbenzene (DVB, 55% isomer, Aldrich), 120mg of V65B free radical initiator (Wako), 10mg of Hydroquinone inhibitor (HQ, Aldrich), 20 mL of 1% polyvinyl alcohol solution (PVA, 87-89% hydrolyzed, Aldrich) for 24h and then polymerized at 70 °C for 15 h in a shaker bath operating at 120 rpm. The resulting crosslinked PS (CLPS) spheres were 700 nm.

The CLPS were coated uniformly with hydrophilic coating of acrylic acid (AA), dialyzed for 48 h, titrated to a pH of roughly 6. Coated CLPS were again swollen with styrene and DVB55 (5 vol %) and polymerized at 70 °C for 15 h. The obtained dumbbell shaped particles were again coated with AA, swollen following the same procedure, polymerized at 70 °C for 15 h and washed.

Sample Preparation

76 mg of particles were coated with FITC (fluorescein isothiocyanate) incorporated in silica. The silica coated particles were treated with solution of polyvinylpyrrolidone in ethanol. A confinement cell was prepared using a 22 x 50 mm glass coverslip (VWR, No. 1 $\frac{1}{2}$) glued onto a large microscope slide. Another coverslip was adhered to the top, and was propped up on one end with cured UV glue dots to define the wedge profile. Silica coated particles dispersed in PVP solution were introduced into

the open end of the confinement cell. The cell was sealed with epoxy and tilted at an angle of 80° from horizontal. The particles were allowed to sediment. After sufficient densification the cell was laid horizontal and equilibrium was re-established. The particle behavior in the confinement cell was observed using confocal and optical microscopes.

System Characterization

SEM images were calculated using a LEO 1550 field emission scanning electron microscope at 1.0 KV. A drop of dilute sample suspension was dried on an aluminum stub and sputtered with gold before taking SEM images. Confocal data was collected using a Zeiss LSM 5 LIVE inverted laser scanning confocal microscope. An excitation wavelength of 600 nm was used. Optical micrographs were collected using a Zeiss LSM optical microscope.

REFERENCES

1. Yablonovitch, E.; Gmitter, T. J., Photonic Band Structure: The Face Centered Cubic Case. *Physical Review Letters* **1989**, 63, (18), 1950-1953.
2. Joannopoulos, J. D.; Maede, R. D.; Winn, J. N., *Photonic Crystals*. Princeton University Press: Princeton, NJ, 1995.
3. Lopez, C., Materials Aspects of Photonic Crystals. *Advanced Materials* **2003**, 15, (20), 1679-1704.
4. Xia, Y.; Gates, B.; Li, Z., Self-Assembly Approaches to Three Dimensional Photonic Crystals. *Advanced Materials* **2001**, 13, (6), 409-413.
5. Tarhan, I. I.; Watson, G. H., Photonic band structure of FCC colloidal crystal. *Physical Review Letters* **1995**, 26, (2), 315-318.
6. Wojciechowski, K. W., Solid Phases of Two-Dimensional Hard Dumb-Bells in the Free Volume Approximation: Crystal-Aperiodic-Solid Phase Transition. *Physics Letters A* **1987**, 122, 377-387.
7. Bates, M. A.; Frenkel, D., Phase behavior of two-dimensional hard rod fluids. *Journal of Chemical Physics* **2000**, 112, 10034-10041.
8. Schilling, T.; Pronk, S.; Mulder, B.; Frenkel, D., Monte Carlo study of hard pentagons. *Physical Review E* **2005**, 71, 036138.
9. Champion, J. A.; Katare, Y. K.; Mitragotri, S., Making Polymeric Micro and Nano-particles of Complex Shapes. *Proceedings of the National Academy of Sciences* **2007**, 104, (29), 11901-11904.
10. Sugimoto, T.; Muramatsu, A.; Sakata, K.; Shindo, D., Characterization of Hematite Particles of Different Shapes. *Journal of Colloid and Interface Science* **1993**, 158, 420-428.
11. Xu, C.; Wang, Q.; Xu, H.; Xie, S.; Yang, Z., General Synthesis of Hollow Composite Ellipsoids. *Colloid Polymer Science* **2007**, 285, 1471-1478.

12. Kim, J.; Larsen, R. J.; Weitz, D. A., Highly Porous Fibers by Electrospinning into a Cryogenic Liquid. *Journal of American Chemical Society* **2006**, 128, (5), 1436-1437.
13. Mock, E. B.; Hank, D. B.; Hawckett, B. S.; Gilbert, R. G.; Zukoski, C. F., Synthesis of Anisotropic Nanoparticles by Seeded Emulsion Polymerization. *Langmuir* **2006**, 22, (9), 4037-4043.
14. Okubo, M.; Minami, H.; Morikawa, K., Production of micron-sized, monodisperse, transformable rugby-ball-like-shaped polymer particles. *Colloid and Polymer Science* **2001**, 279, (9), 931-935.
15. Okubo, M.; Minami, H., Production of micron-sized monodispersed anomalous polymer particles having red blood corpuscle shape *Macromolecular Symposia* **2000**, 150, (1), 201-210.
16. Kim, J.; Larsen, R. J.; Weitz, D. A., Uniform Nonspherical Colloidal Particles with Tunable Shapes. *Advanced Materials* **2007**, 19, (15), 2005-2009.
17. Cho, Y.; Yi, G.; Kim, S.; Jeon, S.; Elsesser, M. T.; Yu, H. K.; Yang, S.; Pine, D. J., Particles with Coordinated Patches or Windows from Oil-in-Water Emulsions. *Chemistry of Materials* **2009**, 19, 3183-3193.
18. Snyder, C.; Yake, A. M.; Feick, J. D.; Velegol, D., Nanoscale Functionalization and Site-Specific Assembly of Colloids by Particle Lithography. *Langmuir* **2005**, 21, 4813-4815.
19. Dendukuri, D.; Pregibon, D. C.; Collins, J.; Hatton, T. A.; Doyle, P. S., Continuous-flow lithography for high-throughput microparticle synthesis. *Nature Materials* **2006**, 5, 365-369.
20. Hosein, I. D.; Liddell, C. M., Homogeneous, Core-Shell, and Hollow-Shell ZnS Colloid-Based Photonic Crystals. *Langmuir* **2007**, 23, 2892-2897.
21. Yin, Y.; Xia, Y., Self-Assembly of Monodispersed Spherical Colloids into Complex Aggregates with Well-Defined Sizes, Shapes, and Structures. *Advanced Materials* **2001**, 13, 267-271.

22. Caruso, R. A.; Susha, A.; Caruso, F., Multilayered Titania, Silica, and Laponite Nanoparticle Coatings on Polystyrene Colloidal Templates and Resulting Inorganic Hollow Spheres. *Chemistry of Materials* **2001**, 13, 400-409.
23. Lee, S. H.; Fung, E. Y.; Riley, E. K.; Liddell, C. M., Asymmetric Colloidal Dimers under Quasi-Two-Dimensional Confinement. *Langmuir* **2009**, 25, 7193-7195.
24. Zhang, J.; Chen, Z.; Whang, Z.; Zhang, W.; Ming, N., Preparation of monodisperse polystyrene spheres in aqueous alcohol system. *Materials Letters* **2003**, 57, (28), 4466-4470.
25. Reece, C.; Guerrero, C. D.; Weissmann, J. M.; Lee, K.; Asher, S. A., Synthesis of Highly Charged, Monodisperse Polystyrene Colloidal Particles for the Fabrication of Photonic Crystals. *Journal of Colloid and Interface Science* **2000**, 232, (1), 76-80.
26. Minami, H.; Wang, Z.; Yamashita, T.; Okubo, M., Thermodynamic analysis of the morphology of monomer-adsorbed, cross-linked polymer particles prepared by the dynamic swelling method and seeded polymerization. *Colloid and Polymer Science* **2003**, 281, (3), 246-252.
27. Graf, C.; Vossen, D.; Imhof, A.; van Blaaderen, A., A General Method to Coat Colloidal Particle with Silica. *Langmuir* **2003**, 19.
28. Camp, P. J.; Duncan, P. D., Two-dimensional structure in a generic model of triangular proteins and protein trimers. *Physical Review E* **2006**, 73, 046111.
29. Oling, F.; Schutter, W.; Brisson, A., Trimers, Dimers of Trimers, and Trimers of Trimers Are Common Building Blocks of Annexin A5 Two-Dimensional Crystals. *Journal of Structural Biology* **2001**, 133, 55-63.
30. Wojciechowski, K. W.; Brańka, A. C.; Frenkel, D., Monte Carlo simulations of a two-dimensional hard dimer system. *Physica A: Statistical Mechanics and its Applications* **1993**, 196, (4), 519-545.
31. Okubo, M.; Minami, H., Control of hollow size of micron-sized monodispersed polymer particles having a hollow structure. *Colloid and Polymer Science* **1996**, 274, (5), 433-438.

32. Okubo, M.; Minami, H., Formation mechanism of micron-sized monodispersed polymer particles having a hollow structure. *Colloid and Polymer Science* **1997**, 275, 992-997.
33. Tissot, I.; Novat, C.; Lefebvre, F.; Bourgeat-Lami, E., Hybrid Latex Particles Coated with Silica. *Macromolecules* **2001**, 34, 5737-5739.
34. Colver, P. J.; Colard, C. A. L.; Bon, S. A. F., Multilayered Nanocomposite Polymer Colloids Using Emulsion Polymerization Stabilized by Solid Particles. *Journal of the American Chemical Society* **2008**, 130, 16850-16851.
35. Balazcs, A. C.; Emrikk, T.; Russel, T. P., Nanoparticle Polymer Composites: Where Two Small Worlds Meet Anna. *Science* **2006**, 314, 1107-1110.
36. Garcia-Celda, L. A.; Chapa-Rodriguez, R.; Bonilla-Rios, J., In situ synthesis of iron oxide nanoparticles in a styrenedivinylbenzene copolymer. *Polymer Bulletin* **2007**, 58, 989-994.
37. Hwang, D. K.; Dendukuri, D.; Doyle, P. S., Microfluidic-based synthesis of non-spherical magnetic hydrogel microparticles. *Lab on a Chip* **2008**, 8, 1640-1647.